A Contour Integral Representation for the Dual Five-Point Function and a Symmetry of the Genus Four Surface in $\mathbb{R}^6$

Andrew J. Hanson and Ji-Ping Sha *
Computer Science Dept. and Mathematics Dept.
Indiana University
Bloomington, IN 47405 USA

February 3, 2008

Abstract

The invention of the "dual resonance model" N-point functions B_N motivated the development of current string theory. The simplest of these models, the four-point function B_4, is the classical Euler Beta function. Many standard methods of complex analysis in a single variable have been applied to elucidate the properties of the Euler Beta function, leading, for example, to analytic continuation formulas such as the contour-integral representation obtained by Pochhammer in 1890. However, the precise features of the expected multiple-complex-variable generalizations to B_N have not been systematically studied. Here we explore the geometry underlying the dual five-point function B_5, the simplest generalization of the Euler Beta function. The original integrand defining B_5 leads to a polyhedral structure for the five-crosscap surface, embedded in $\mathbb{R}\mathbf{P}^5$, that has 12 pentagonal faces and a symmetry group of order 120 in $\mathbf{PGL}(6)$. We find a Pochhammer-like representation for B_5 that is a contour integral along a surface of genus five in $\mathbb{C}\mathbf{P}^2\#4\overline{\mathbb{C}\mathbf{P}^2}$. The symmetric embedding of the five-crosscap surface in $\mathbb{R}\mathbf{P}^5$ is doubly covered by a corresponding symmetric embedding of the surface of genus four in $\mathbf{S}^5 \subset \mathbb{R}^6$ that has a polyhedral structure with 24

*Email: {hansona, jsha}@indiana.edu

pentagonal faces and a symmetry group of order 240 in $\mathbf{O}(6)$. These symmetries enable the construction of elegant visualizations of these surfaces. The key idea of the paper is to realize that the compactification of the set of five-point cross-ratios forms a smooth real algebraic subvariety that is the five-crosscap surface in $\mathbb{R}\mathbf{P}^5$. It is in the complexification of this surface that we construct the contour integral representation for B_5. Our methods are generalizable in principle to higher dimensions, and therefore should be of interest for further study.

1 Introduction

Historical Background. In 1968, Gabriele Veneziano [18] noticed that an amazing number of abstract properties required by the relativistic scattering amplitude for four colliding spinless particles were embodied in the classical Euler Beta function, $B(\alpha_1, \alpha_2)$, which can be defined by the integral representation

$$B(\alpha_1, \alpha_2) = \int_0^1 x^{\alpha_1 - 1}(1-x)^{\alpha_2 - 1}\, dx\ , \quad \mathrm{Re}\,\alpha_1 > 0,\ \mathrm{Re}\,\alpha_2 > 0\ . \tag{1}$$

This observation served as the implausible origin of modern string theory (see, e.g., [13, 14] for more details), which grew from the discovery that the Beta function could be related to the vibration modes of a relativistic string sweeping out a surface in spacetime [4, 11].

Almost immediately following Veneziano's discovery, a function with a two-dimensional integral representation was found that could be related to the relativistic scattering amplitude of *five* spinless particles [1, 19]. This function, the dual five-point function B_5, can be written in various representations such as the following integral over a triangular region

$$\begin{aligned} &B_5(\alpha_1, \alpha_2, \alpha_3, \alpha_4, \alpha_5) = \\ &\quad = \iint\limits_{0<y<x<1} x^{\alpha_1 - \alpha_2 - \alpha_5} y^{\alpha_2 - 1}(1-x)^{\alpha_3 - 1}(x-y)^{\alpha_5 - 1}(1-y)^{\alpha_4 - \alpha_3 - \alpha_5}\, dx\, dy \end{aligned} \tag{2}$$

for suitably restricted values of the arguments $(\alpha_1, \alpha_2, \alpha_3, \alpha_4, \alpha_5)$. The discovery of this function indicated that the Euler Beta function was not alone: the Euler Beta function, which would now be written as $B_4(\alpha_1, \alpha_2)$, was henceforth to be regarded as the first member of the family of N-point functions B_N that might be expected to have interesting properties in analysis as well as in the quantum theory of relativistic elementary particles.

Cross-Ratio Coordinates. A very rapid series of steps subsequently led to what became the standard Koba-Nielsen representation [10] for the N-point function $B_N(\alpha_{13}, \ldots, \alpha_{N-2,N})$, which can be written as an $(N-3)$-dimensional integral

$$B_N(\alpha_{13}, \ldots, \alpha_{N-2,N}) = \int \cdots \int_{0<t_1<\cdots<t_{N-3}<1} \prod_{i,j} {u_{ij}}^{\alpha_{ij}-1} d\mu_N \ , \tag{3}$$

where $d\mu_N = dt_1 \cdots dt_{N-3} / \prod_{i=1}^{N-4} t_i \prod_{j=2}^{N-3} (1-t_j)$ and the u_{ij} are the N-point cross-ratios parameterized by $t_1, \ldots, t_{N-3}$ as described in detail in Section 2. The formulas (1) and (2) correspond to (3) for the cases $N = 4$ and $N = 5$, respectively.

A variety of methods have been employed to study the properties of the B_N integrands as functions of complex variables. For example, Koba and Nielson [10] expressed (3) as an integral in a space that was essentially a product of $(N-3)$ copies of $\mathbb{C}\mathbf{P}^1$. As noted by one of the current authors in [6], one can alternatively express the complex integrand by employing $\mathbb{C}\mathbf{P}^{N-3}$ cross-ratios (with a much larger symmetry group) in place of the product of $(N-3)$ complex projective lines with the single shared linear fractional transformation symmetry characterizing the Koba-Nielsen framework.

We will see in the following that, for B_5, the compactification of the set of all five-point cross-ratios can be identified with $\mathbb{R}\mathbf{P}^2 \# 4\mathbb{R}\mathbf{P}^2$ as an algebraic subvariety in $\mathbb{R}\mathbf{P}^5$ with a polyhedral structure that has 12 pentagonal faces. This embedding of $\mathbb{R}\mathbf{P}^2 \# 4\mathbb{R}\mathbf{P}^2$ has a symmetry group of order 120 in $\mathbf{PGL}(6)$. The double covering, which is the surface of genus four embedded in $\mathbf{S}^5 \subset \mathbb{R}^6$, has a corresponding polyhedral structure with 24 pentagonal faces and a symmetry group of order 240 in $\mathbf{O}(6)$. The integral (2) is taken over one of the 12 pentagonal faces of $\mathbb{R}\mathbf{P}^2 \# 4\mathbb{R}\mathbf{P}^2$. This is the starting point for the contour integral representation of B_5.

The study of such a tessellation on $\mathbb{R}\mathbf{P}^2 \# 4\mathbb{R}\mathbf{P}^2$, the five crosscap surface, and its symmetry group dates back to the 19th century [9] and is treated in detail in the work of Brahana and Coble in 1926 [2]. It is interesting to see that our space of five-point cross-ratios leads naturally to the same tessellation, and to the presentation of the symmetry group in $\mathbf{O}(6)$.

Contour Integral Representations. It is well known that the analytic continuation of the function defined by (1) is a meromorphic function of (α_1, α_2) on the entire complex space $\mathbb{C}^2$. In fact, changing variables in the integral allows the

Beta function to be rewritten in terms of the standard integral representation of the Gamma function, leading to the explicit analytic continuation formula

$$B(\alpha_1, \alpha_2) = \frac{\Gamma(\alpha_1)\Gamma(\alpha_2)}{\Gamma(\alpha_1 + \alpha_2)} \,. \tag{4}$$

In 1890, Pochhammer [12] gave another interesting continuation formula for $B(\alpha_1, \alpha_2)$ in the following form,

$$B(\alpha_1, \alpha_2) = \frac{\epsilon(\alpha_1, \alpha_2)}{(1 - e^{2\pi i \alpha_1})(1 - e^{2\pi i \alpha_2})} \,, \tag{5}$$

where $\epsilon(\alpha_1, \alpha_2)$ is a contour integral of $\beta(z; \alpha_1, \alpha_2) = z^{\alpha_1 - 1}(1 - z)^{\alpha_2 - 1}$ along a properly immersed loop in $\mathbb{C} \setminus \{0, 1\}$, and hence is a holomorphic function of (α_1, α_2).

Our observation that the B_5 function can be expressed by an integral over one pentagonal face of $\mathbb{R}\mathbf{P}^2 \# 4\mathbb{R}\mathbf{P}^2$ leads to a contour integral representation analogous to Pochhammer's classic representation of B_4. We obtain the following two-dimensional contour integral representation of B_5:

$$\begin{aligned} &B_5(\alpha_1, \alpha_2, \alpha_3, \alpha_4, \alpha_5) = \\ &\quad = \frac{\epsilon(\alpha_1, \alpha_2, \alpha_3, \alpha_4, \alpha_5)}{(1 - e^{2\pi i \alpha_1})(1 - e^{2\pi i \alpha_2})(1 - e^{2\pi i \alpha_3})(1 - e^{2\pi i \alpha_4})(1 - e^{2\pi i \alpha_5})} \,. \end{aligned} \tag{6}$$

Here $\epsilon(\alpha_1, \alpha_2, \alpha_3, \alpha_4, \alpha_5)$ is a holomorphic function expressed as an integral of a holomorphic 2-form along a closed oriented surface of genus 5 properly immersed in $\mathbb{C}\mathbf{P}^2 \# 4\overline{\mathbb{C}\mathbf{P}^2}$. Note that, unlike the representation (2), where $(\alpha_1, \alpha_2, \alpha_3, \alpha_4, \alpha_5)$ must be properly restricted for the integral to be convergent, the representation (6) of B_5 is a meromorphic function of $(\alpha_1, \alpha_2, \alpha_3, \alpha_4, \alpha_5)$ and is defined on the entire space $\mathbb{C}^5$. Hence the formula (6) is an explicit analytic continuation formula for the five-point function B_5 originally defined by (2).

We point out that, to produce the required contour for B_5, not only is the two-complex-variable environment supplied by the Koba-Nielson product of two projective lines, $\mathbb{C}\mathbf{P}^1 \times \mathbb{C}\mathbf{P}^1$, inadequate, but the richer alternative $\mathbb{C}\mathbf{P}^2$ framework of [6] is *also* inadequate. The contour lies instead in $\mathbb{C}\mathbf{P}^2 \# 4\overline{\mathbb{C}\mathbf{P}^2}$, which is the complexification of the above-mentioned five-crosscap surface $\mathbb{R}\mathbf{P}^2 \# 4\mathbb{R}\mathbf{P}^2$ in $\mathbb{R}\mathbf{P}^5$ considered as the real part of $\mathbb{C}\mathbf{P}^5$.

We begin in Section 2 by introducing the N-point cross-ratio, which gives rise to the subvarieties upon which our analysis is based. Section 3 constructs

the 12-pentagon tessellation of the five-crosscap surface as the compactification of the set of 5-point cross-ratios; its symmetries and the genus-four double cover are given in Section 4. Then, in Section 5, we review Pochhammer's classical construction for the contour integral representation of the Euler Beta function. The framework for studying B_5 is set up in Section 6 where the representation (6) is proven. Selected constructions are applied to visualizations and computer graphics representations of the relevant structures in Section 7. Remarks on the extension to general N are presented in Section 8.

2 Cross-Ratios

Recall that the cross-ratio of four distinct ordered numbers $\{w, x, y, z\} \subset \mathbb{R} \cup \{\infty\}$ is defined as

$$u(w,x,y,z) = \frac{(w-y)}{(w-z)} \Big/ \frac{(x-y)}{(x-z)} = \frac{(w-y)(x-z)}{(w-z)(x-y)} \,. \tag{7}$$

For any integer $N \geq 4$, we define the *N-point cross-ratio* of a cyclically-ordered set of N distinct numbers $\{x_1, \ldots, x_N\} \subset \mathbb{R} \cup \{\infty\}$ as the ordered set of $N(N-3)/2$ numbers $(u_{13}, u_{14}, \ldots, u_{N-2,N})$, where

$$u_{ij} \;=\; u(x_i, x_{i+1}, x_{j+1}, x_j) = \frac{(x_i - x_{j+1})(x_{i+1} - x_j)}{(x_i - x_j)(x_{i+1} - x_{j+1})} \tag{8}$$

and $1 \leq i < j \leq N$, $2 \leq j - i \leq N - 2$.

The set of all N-point cross-ratios can be considered as a subset of $\mathbb{R}^{N(N-3)/2}$, which we denote by $\mathcal{C}$. From the well-known fact that the cross-ratio is invariant under linear fractional transformations of $\mathbb{R} \cup \{\infty\}$, it is clear that $\mathcal{C}$ can be parameterized by $(N-3)$ variables, which we denote as $(t_1, \ldots, t_{N-3})$. That is, each point of $\mathcal{C}$ is the N-point cross-ratio of the N cyclically ordered numbers

$$\{0, \infty, 1, t_1, \ldots, t_{N-3}\}, \tag{9}$$

for a unique $(t_1, \ldots, t_{N-3}) \in \mathbb{R}^{N-3}$, where $t_1, \ldots, t_{N-3}$ are distinct and not equal to 0 or 1.

For example, for $N = 4$, if we set $x_1 = 0$, $x_2 = \infty$, $x_3 = 1$, and $x_4 = t$, then, according to (8), the set of 4-point cross-ratios in $\mathbb{R}^2$ is given by the following parameterized curve:

$$\begin{aligned} u_{13} \;&=\; u(x_1, x_2, x_4, x_3) = u(0, \infty, t, 1) = t \\ u_{24} \;&=\; u(x_2, x_3, x_1, x_4) = u(\infty, 1, 0, t) = 1 - t \,. \end{aligned}$$

Notice that there are three connected components for the domain of t, as shown in Figure 1.

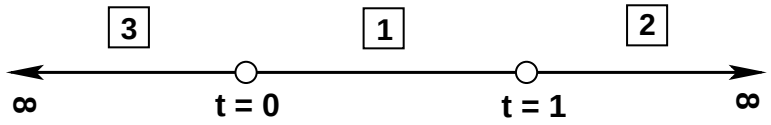

Figure 1: The 3 connected components of the domain of the parameters for the set of 4-point cross-ratios.

For $N = 5$, the set of 5-point cross-ratios is a surface in $\mathbb{R}^5$ parameterized by (s, t) as

$$\begin{aligned} u_{13} &= u(x_1, x_2, x_4, x_3) = u(0, \infty, s, 1) = s \\ u_{14} &= u(x_1, x_2, x_5, x_4) = u(0, \infty, t, s) = \frac{t}{s} \\ u_{24} &= u(x_2, x_3, x_5, x_4) = u(\infty, 1, t, s) = \frac{1-s}{1-t} \\ u_{25} &= u(x_2, x_3, x_1, x_5) = u(\infty, 1, 0, t) = 1 - t \\ u_{35} &= u(x_3, x_4, x_1, x_5) = u(1, s, 0, t) = \frac{s-t}{s(1-t)} \, . \end{aligned} \tag{10}$$

The domain of (s, t) has twelve connected components, as shown in Figure 2.

One can verify that the cross-ratios u_{ij} defined by (8) satisfy

$$u_{ij} = 1 - \prod_{m=i+1}^{j-1} \prod_{n=j+1}^{i-1} u_{mn} \tag{11}$$

with the convention that $u_{mn} = u_{nm}$ and $u_{m,n+N} = u_{m,N}$ for all $1 \leq m, n \leq N$. In fact, the affine algebraic subvariety in $\mathbb{R}^{N(N-3)/2}$ defined by (11), minus a set of measure zero, is precisely the set $\mathcal{C}$ of N-point cross-ratios.

In particular, for $N = 4$, the constraint (11) becomes

$$u_{13} = 1 - u_{24} \, . \tag{12}$$

The set $\mathcal{C}$ is the affine algebraic subvariety in $\mathbb{R}^2$ with coordinates $(z_1, \, z_2)$ given by the linear equation

$$1 - z_1 - z_2 = 0 \, . \tag{13}$$

For $N = 5$, we have

$$\begin{aligned} u_{13} &= 1 - u_{24}\, u_{25} \\ u_{14} &= 1 - u_{25}\, u_{35} \\ u_{24} &= 1 - u_{35}\, u_{13} \\ u_{25} &= 1 - u_{13}\, u_{14} \\ u_{35} &= 1 - u_{14}\, u_{24}\ , \end{aligned} \tag{14}$$

and $\mathcal{C}$ is the affine algebraic subvariety in $\mathbb{R}^5$ with coordinates $(z_1, z_2, z_3, z_4, z_5)$ given by

$$\begin{aligned} 1 - z_1 - z_3 z_4 &= 0 \\ 1 - z_2 - z_4 z_5 &= 0 \\ 1 - z_3 - z_5 z_1 &= 0 \\ 1 - z_4 - z_1 z_2 &= 0 \\ 1 - z_5 - z_2 z_3 &= 0\ . \end{aligned} \tag{15}$$

Remark. It can be verified that the system (15) has rank 3 at the zero locus, and therefore does actually define a smooth algebraic subvariety of dimension 2.

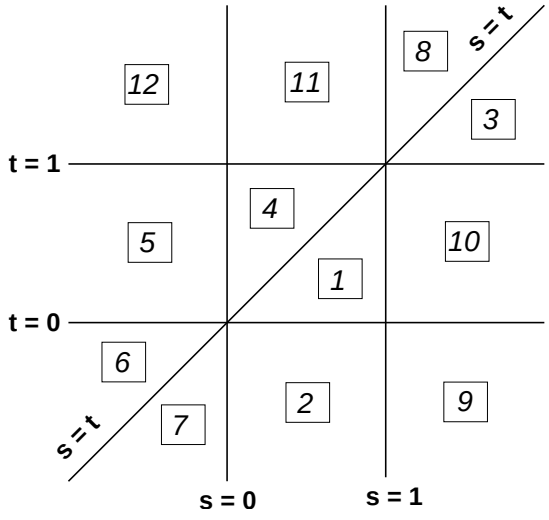

Figure 2: The 12 connected components of the domain of parameters for the set of 5-point cross-ratios.

Now consider the corresponding projective subvarieties. For $N = 4$, (13) becomes

$$z_0 - z_1 - z_2 = 0 \,, \tag{16}$$

which obviously defines a projective line in $\mathbb{R}\mathbf{P}^2$ with homogeneous coordinates $[z_0, z_1, z_2]$.

Similarly, for $N = 5$, (15) yields the following homogeneous quadratic equations in the homogeneous coordinates $[z_0, z_1, z_2, z_3, z_4, z_5]$ of $\mathbb{R}\mathbf{P}^5$:

$$\begin{aligned} {z_0}^2 - z_0 z_1 - z_3 z_4 &= 0 \\ {z_0}^2 - z_0 z_2 - z_4 z_5 &= 0 \\ {z_0}^2 - z_0 z_3 - z_5 z_1 &= 0 \\ {z_0}^2 - z_0 z_4 - z_1 z_2 &= 0 \\ {z_0}^2 - z_0 z_5 - z_2 z_3 &= 0 \,. \end{aligned} \tag{17}$$

One can verify that (17) defines a smooth two-dimensional subvariety in $\mathbb{R}\mathbf{P}^5$, which we will denote by M. To see the topology of M, we examine the parameterization (10). As we will show in detail in Section 3, the image of each of the twelve connected components of the parameter domain has a smooth pentagonal closure tessellating M as shown in Figure 3. Extending (17) to complex variables defines a complex algebraic variety M^c that is obviously the complexification of the real manifold M. M^c is $\mathbb{C}\mathbf{P}^2$ with four points blown up and is topologically homeomorphic to $\mathbb{C}\mathbf{P}^2 \# 4\overline{\mathbb{C}\mathbf{P}^2}$.

The tessellation represented in Figure 3 has 12 pentagonal faces, $(12 \times 5)/2 = 30$ edges, and $(12 \times 5)/4 = 15$ vertices; the Euler number of M is thus $\chi = 15 - 30 + 12 = -3$, and therefore M is the connected sum of five $\mathbb{R}\mathbf{P}^2$'s, i.e., a sphere with five crosscaps. Therefore, viewing the five-crosscap surface as the set of cross-ratios yields a natural tessellation with 12 pentagonal faces, which we can call a "dodecahedron" even though it does not bound a 3-ball. This tessellation was already described in detail from the point of view of combinatorial topology in the 19th century [9]. In 1926, Brahana and Coble [2], also arrived at the same tessellation of a sphere with five crosscaps as a map of 12 countries with five sides, and studied the symmetry group in detail (see also recent work by Weber [20] for additional historical background). Such tessellations were generalized by Stasheff for use in his study of the homotopy theory of H-spaces [15–17], and, in particular, the analogous tiles in higher dimensions are called associahedra. These have played a prominent role, e.g., in the work of Devadoss [3]. Our discovery of the relation between the five-crosscap dodecahedral tessellation and the 5-point cross-

ratios, as well as the apparent relation between the higher-dimensional analogs and the N-point cross-ratios, should thus be of further interest.

3 Closure of the 5-Point Cross-Ratio Set in $\mathbb{R}\mathbf{P}^5$

We now present a detailed treatment of the pentagonal tessellation for M. In the homogeneous coordinates of $\mathbb{R}\mathbf{P}^5$, we will write the parameterization (10) as

$$\begin{aligned} p(s,t) &= \left[1, s, \frac{t}{s}, \frac{1-s}{1-t}, (1-t), \frac{s-t}{s(1-t)}\right] \\ &= \left[s(1-t), s^2(1-t), t(1-t), s(1-s), s(1-t)^2, s-t\right] \ . \end{aligned} \tag{18}$$

On the triangular connected component $0 < t < s < 1$, as $(s,t) \to (0,0)$ or $(s,t) \to (1,1)$, the images do not converge to a point. To extend the parameterization to the boundary of the domain, we will replace the parameters (s,t) as follows.

First, let

$$(x,y) = \begin{cases} (2u - uv,\ uv), & \text{for } 0 < u \le \frac{1}{2},\ 0 < v < 1 \\ (1 - v + uv,\ -1 + 2u + v - uv), & \text{for } \frac{1}{2} \le u < 1,\ 0 < v < 1. \end{cases} \tag{19}$$

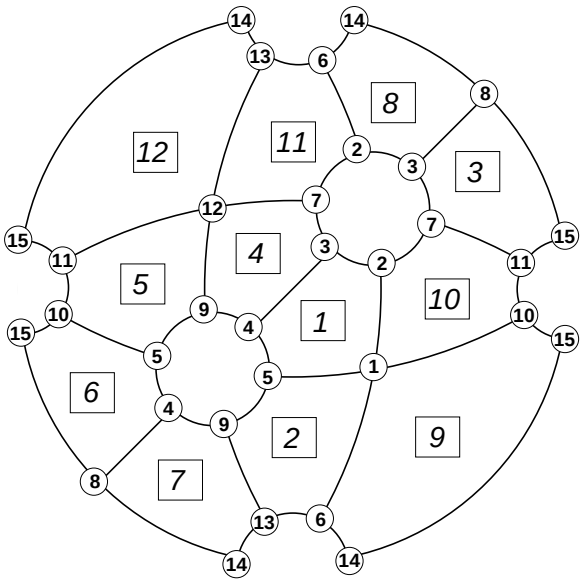

Figure 3: The pentagonal tessellation of the closure of the set of 5-point cross-ratios.

The formula (19) defines a 1-1 map between the open square $(0,1)\times(0,1)$ in the uv-plane and the open triangle $0<y<x<1$ in the xy-plane, as shown in Figure 4.

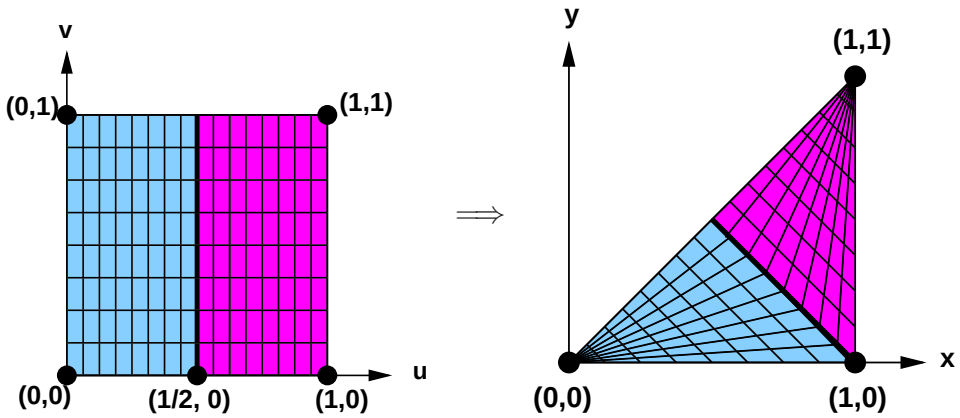

Figure 4: The map from the square $0<u,v<1$ in the uv-plane to the triangular region $0<y<x<1$ in the xy-plane.

Next, in Table 1, we present twelve formulas that give 1-1 maps between the open triangular domain $0<y<x<1$ and each of the twelve connected components shown in Figure 2.

Composing (18), the entries in Table 1, and (19), we get a parameterization for each of the 12 connected components of $\mathcal{C}$ on the common domain $(0,1)\times(0,1)$ in the uv-plane. We will denote these parameterizations by $f_1,\ldots,f_{12}$, respectively.

It can be verified that each of the $f_1,\ldots,f_{12}$ extends as a 1-1 parameterization to the closed square $[0,1]\times[0,1]$. Each of the twelve images is a smooth, closed, pentagonal surface patch whose vertices correspond to

$$(u,v)=(\tfrac{1}{2},0),\ (1,0),\ (1,1),\ (0,1),\ (0,0)\ .$$

Examining the pentagons one by one, we find they are joined together to form the closed surface represented by Figure 3.

For future reference, we list below the homogeneous coordinates of the 15

n	The map from the region $0 < y < x < 1$ to the connected component $\boxed{n}$ in Figure 2.
1	$s = x$, $t = y$
2	$s = (x-y)/(1-y)$, $t = y/(y-1)$
3	$s = 1/(xy)$, $t = x/y$
4	$s = y$, $t = x$
5	$s = y/(y-1)$, $t = (x-y)/(1-y)$
6	$s = x/(x-1)$, $t = (x-y)/(x-1)$
7	$s = (x-y)/(x-1)$, $t = x/(x-1)$
8	$s = x/y$, $t = 1/(xy)$
9	$s = (1-y)/(x-y)$, $t = y/(y-x)$
10	$s = 1/(1-y)$, $t = (1-x)/(1-y)$
11	$s = (1-x)/(1-y)$, $t = 1/(1-y)$
12	$s = y/(y-x)$, $t = (1-y)/(x-y)$

Table 1: Transformations from the triangular region $0 < y < x < 1$ to the 12 connected components in Figure 2.

---

vertices:

$$
\begin{aligned}
v_1 &= [1, 1, 0, 0, 1, 1] & \qquad v_9 &= [0, 0, 1, 0, 0, -1] \\
v_2 &= [1, 1, 1, 0, 0, 1] & v_{10} &= [0, -1, 0, 1, 0, 0] \\
v_3 &= [1, 1, 1, 1, 0, 0] & v_{11} &= [0, 0, 0, 1, 0, 0] \\
v_4 &= [1, 0, 1, 1, 1, 0] & v_{12} &= [0, 0, 0, 0, 0, 1] \\
v_5 &= [1, 0, 0, 1, 1, 1] & v_{13} &= [0, 0, 1, 0, 0, 0] \\
v_6 &= [0, 0, -1, 0, 1, 0] & v_{14} &= [0, 0, 0, 0, 1, 0] \\
v_7 &= [0, 0, 0, -1, 0, 1] & v_{15} &= [0, 1, 0, 0, 0, 0]\,. \\
v_8 &= [0, 1, 0, 0, -1, 0]
\end{aligned}
\tag{20}
$$

4 Symmetries and the Double-Covering Lift

One can see using combinatorial arguments that the tessellation of M shown in Figure 3 has many symmetries. We will present the group of symmetries as follows.

One of the symmetries, when restricted to face $\boxed{1}$, is a rotation that transforms the vertices 1,2,3,4,5 to 2,3,4,5,1. This symmetry also transforms vertex 12 to

vertex 15. Using the coordinates of these vertices from (20), we construct the matrix

$$X_5 = B \cdot A^{-1}$$

with A the 6×6 matrix given by $A = [v_1\, v_2\, v_3\, v_4\, v_5\, v_{12}]$, where v_1, etc., are written as column vectors whose components are specified by (20). Similarly, $B = [v_2\, v_3\, v_4\, v_5\, v_1\, v_{15}]$, yielding

$$X_5 = \begin{bmatrix} 1 & 0 & 0 & 0 & 0 & 0 \\ 0 & 0 & 1 & 0 & 0 & 0 \\ 0 & 0 & 0 & 1 & 0 & 0 \\ 0 & 0 & 0 & 0 & 1 & 0 \\ 0 & 0 & 0 & 0 & 0 & 1 \\ 0 & 1 & 0 & 0 & 0 & 0 \end{bmatrix}, \tag{21}$$

Another symmetry is the reflection along the edge joining v_3 and v_4, which transforms vertices 1,2,3,4,5,12 to 12,7,3,4,9,1. As above, one constructs

$$X_2 = \begin{bmatrix} 1 & 0 & 0 & 0 & 0 & -1 \\ 2 & 0 & -1 & 0 & -1 & -1 \\ 0 & 0 & 0 & 1 & 0 & 0 \\ 0 & 0 & 1 & 0 & 0 & 0 \\ 2 & -1 & 0 & -1 & 0 & -1 \\ 0 & 0 & 0 & 0 & 0 & -1 \end{bmatrix}. \tag{22}$$

The following observations are essential: Viewing X_5 and X_2 as elements of $\mathbf{PGL}(6)$, one can verify that the zero-locus of (17) is invariant under the corresponding transformations of $\mathbb{R}\mathbf{P}^5$. X_5 and X_2 generate a group of order 120, which is isomorphic to the group of automorphisms of M mentioned above. In other words, we have embedded the automorphism group of M in $\mathbf{PGL}(6)$.

In fact, X_5 and X_2 generate a subgroup G of order 120 in $\mathbf{GL}(6)$. We let

$$Q = \frac{1}{70} \sum_{g \in G} (g)^t \cdot g\ . \tag{23}$$

More explicitly,

$$Q = \begin{bmatrix} 20 & -6 & -6 & -6 & -6 & -6 \\ -6 & 4 & 1 & 2 & 2 & 1 \\ -6 & 1 & 4 & 1 & 2 & 2 \\ -6 & 2 & 1 & 4 & 1 & 2 \\ -6 & 2 & 2 & 1 & 4 & 1 \\ -6 & 1 & 2 & 2 & 1 & 4 \end{bmatrix}. \tag{24}$$

As is well-known, Q defines a G-invariant quadratic form on $\mathbb{R}^6$. Then the algebraic subvariety in $\mathbb{R}^6$ defined by

$$\begin{aligned} {z_0}^2 - z_0 z_1 - z_3 z_4 &= 0 \\ {z_0}^2 - z_0 z_2 - z_4 z_5 &= 0 \\ {z_0}^2 - z_0 z_3 - z_5 z_1 &= 0 \\ {z_0}^2 - z_0 z_4 - z_1 z_2 &= 0 \\ {z_0}^2 - z_0 z_5 - z_2 z_3 &= 0 \\ [z_0\, z_1\, z_2\, z_3\, z_4\, z_5] \cdot Q \cdot [z_0\, z_1\, z_2\, z_3\, z_4\, z_5]^t &= 1 \end{aligned} \tag{25}$$

is G-invariant and we denote it by $\widetilde{M}$.

Comparing to (17), we see that $\widetilde{M}$ is the double covering of M lifted from $\mathbb{R}\mathbf{P}^5$ to $\mathbb{R}^6$ and is therefore topologically the orientable surface of *genus four*. Notice that $\widetilde{M}$ is also invariant under the action of $-I_6$, where I_6 denotes the 6×6 identity matrix. Hence, $\widetilde{M}$ is invariant under the group $\widetilde{G}$ generated by X_5, X_2, and $-I_6$, which has 240 elements in $\mathbf{GL}(6)$.

Let P be a 6×6 matrix satisfying

$$P^t P = Q\,. \tag{26}$$

Then $P\widetilde{M} \subset \mathbf{S}^5$, where $\mathbf{S}^5 = \{(x_0, \ldots, x_5) \in \mathbb{R}^6 \,:\, {x_0}^2 + \cdots + {x_5}^2 = 1\}$ is the unit sphere in $\mathbb{R}^6$, and it is invariant under the subgroup of order 240 in $\mathbf{O}(6)$ generated by PX_5P^{-1}, PX_2P^{-1}, and $-I_6$.

With the parameterization $f_1(u,v), \ldots, f_{12}(u,v)$ for M from Section 3, we can now easily write down the following parameterization for $\widetilde{M}$:

$$\tilde{f}_i^{\pm} = \frac{\pm f_i}{\sqrt{f_i^t \cdot Q \cdot f_i}} \quad i = 1, \ldots, 12\,. \tag{27}$$

Each $\tilde{f}_i^{\pm}$ maps $[0,1] \times [0,1]$ in the uv-plane to a pentagonal surface patch. This yields a tessellation of $\widetilde{M}$ with 24 pentagonal faces. As mentioned at the end of Section 2, such a tessellation for the genus-four surface has long been known. Here we have performed this tessellation symmetrically in $\mathbb{R}^6$.

The coordinates of the vertices appearing in the tessellation of $\widetilde{M}$ can be computed from (27) at the points $(u,v) = (\frac{1}{2}, 0)$, $(1,0)$, $(1,1)$, $(0,1)$, $(0,0)$. They are in fact the same as those presented in (20), together with their negatives, viewed now as coordinates in $\mathbb{R}^6$.

We now identify the 24 faces in $\widetilde{M}$ with ordered sets of vertices in $\mathbb{R}^6$: the oriented faces are labeled in terms of the indices of the vertices in (20), where a minus sign indicates the negative mirror vertex and conjugate faces are denoted with bars:

$$
\begin{array}{llll}
\text{face } 1: & (1,2,3,4,5) & \text{face } \bar{1}: & (-1,-5,-4,-3,-2) \\
\text{face } 2: & (1,5,-9,-13,6) & \text{face } \bar{2}: & (-1,-6,+13,+9,-5) \\
\text{face } 3: & (8,15,11,-7,3) & \text{face } \bar{3}: & (-8,-3,+7,-11,-15) \\
\text{face } 4: & (-12,9,4,3,-7) & \text{face } \bar{4}: & (12,7,-3,-4,-9) \\
\text{face } 5: & (12,-9,5,10,11) & \text{face } \bar{5}: & (-12,-11,-10,-5,9) \\
\text{face } 6: & (-8,-15,10,5,4) & \text{face } \bar{6}: & (+8,-4,-5,-10,+15) \\
\text{face } 7: & (-8,4,9,13,14) & \text{face } \bar{7}: & (+8,-14,-13,-9,-4) \\
\text{face } 8: & (8,3,2,-6,-14) & \text{face } \bar{8}: & (-8,+14,+6,-2,-3) \\
\text{face } 9: & (1,6,14,15,-10) & \text{face } \bar{9}: & (-1,+10,-15,-14,-6) \\
\text{face } 10: & (1,-10,-11,7,2) & \text{face } \overline{10}: & (-1,-2,-7,+11,+10) \\
\text{face } 11: & (12,13,-6,2,7) & \text{face } \overline{11}: & (-12,-7,-2,+6,-13) \\
\text{face } 12: & (12,11,15,14,13) & \text{face } \overline{12}: & (-12,-13,-14,-15,-11)\,.
\end{array}
\tag{28}
$$

The correspondence between the 12 projective faces and the 12 (s,t) regions of Figure 2 is shown in Figure 3; the correspondence between the 24 faces in the double cover $\widetilde{M}$ and the 12 regions is shown in Figure 5.

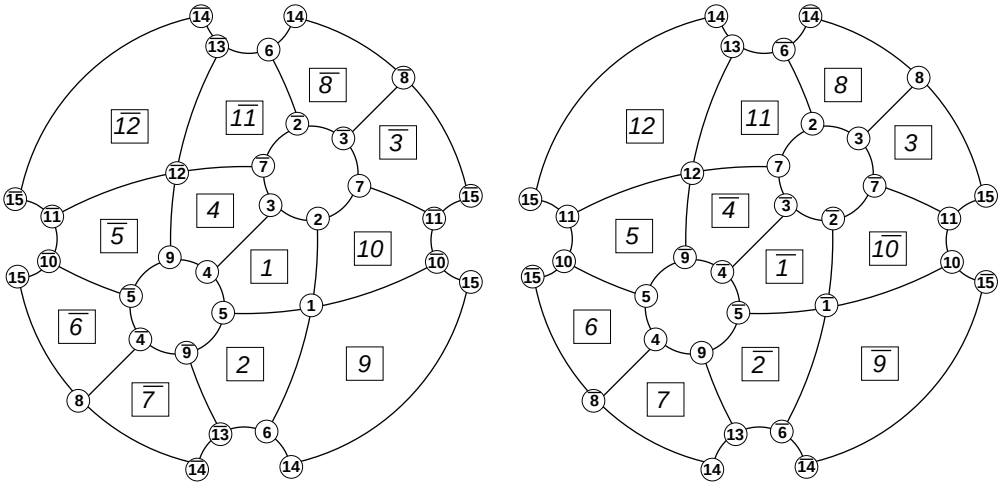

Figure 5: The 24 face identifications of the double covering.

5 Review of the Pochhammer Contour for B_4

In this section, we review Pochhammer's construction [8, 12, 21] of the contour integral leading to the formula (5) for B_4. This will lead us to the contour integral representation for B_5 to be presented in Section 6.

Let

$$\beta(z;\, \alpha_1, \alpha_2) = z^{\alpha_1 - 1}\, (1-z)^{\alpha_2 - 1}\ . \tag{29}$$

where (α_1, α_2) is a pair of arbitrary complex numbers. Considered as a function of z, β defines a family of holomorphic functions on a proper Riemann covering sheaf S over $\mathbb{C} \setminus \{0, 1\}$. Let C be a closed and oriented curve in S that is the lift of the closed and oriented curve in $\mathbb{C} \setminus \{0, 1\}$ shown in Figure 6, where we label the line segments by their relative phases in the lift. This is known as the Pochhammer contour.

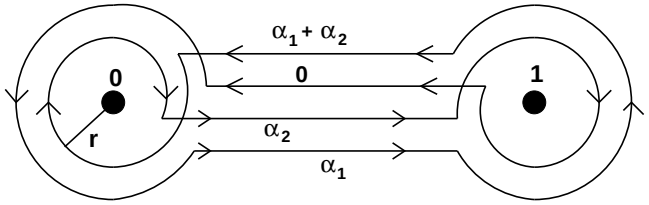

Figure 6: The Pochhammer contour C for the Euler Beta function.

Next, define

$$\epsilon(\alpha_1, \alpha_2) = \int_C \beta(z;\, \alpha_1, \alpha_2)\, dz\ .$$

Clearly $\epsilon(\alpha_1, \alpha_2)$ is a holomorphic function of (α_1, α_2) and is invariant under continuous deformations of C. Therefore, letting $r \to 0^+$ in Figure 6, one easily sees that, if $\mathrm{Re}\, \alpha_1 > 0$ and $\mathrm{Re}\, \alpha_2 > 0$, then

$$\epsilon(\alpha_1, \alpha_2) = (1 - e^{2\pi i \alpha_1})(1 - e^{2\pi i \alpha_2}) \int_0^1 x^{\alpha_1 - 1} (1-x)^{\alpha_2 - 1}\, dx\ ,$$

which yields the formula (5).

If α_1 (or α_2, resp.) is an integer ≥ 1, then the holomorphic 1-form $\beta(z;\, \alpha_1, \alpha_2)\, dz$ on S descends to a holomorphic 1-form on a proper Riemann covering sheaf over $\mathbb{C} \setminus \{0\}$ (or $\mathbb{C} \setminus \{1\}$, resp.). Since the curve in Figure 6 is contractible in $\mathbb{C} \setminus \{0\}$ (or $\mathbb{C} \setminus \{1\}$, resp.), $\epsilon(\alpha_1, \alpha_2) = 0$.

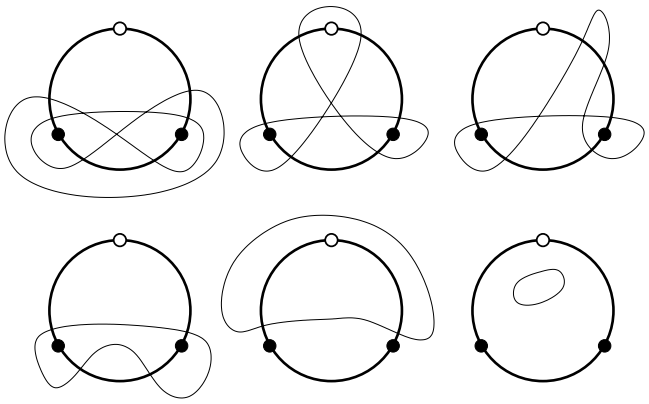

Figure 7: The deformation of the Pochhammer contour to a null contour when the conditions $\alpha_1 + \alpha_2 = 0, -1, -2, \ldots$ remove the branch point at infinity (open circle).

Notice that, by letting $w = 1/z$, we have

$$z^{\alpha_1 - 1}\,(1-z)^{\alpha_2 - 1}\,dz \;= -(w-1)^{\alpha_2 - 1} w^{-\alpha_1 - \alpha_2}\,dw \;\;.$$

This shows that, if $(\alpha_1 + \alpha_2)$ is a non-positive integer ($\alpha_1 + \alpha_2 = 0,\ -1,\ -2, \ldots$), the holomorphic 1-form $\beta(z;\ \alpha_1, \alpha_2)\,dz$ on S descends to a holomorphic 1-form on a proper Riemann covering sheaf over $\mathbb{C}\mathbf{P}^1 \setminus \{0, 1\}$, where as usual we identify $\mathbb{C}\mathbf{P}^1$ with $\mathbb{C} \cup \{\infty\}$. Since the curve in Figure 6 is contractible in $\mathbb{C}\mathbf{P}^1 \setminus \{0, 1\}$ (see Figure 7), it therefore follows that $\epsilon(\alpha_1, \alpha_2) = 0$ also in this case. Figure 7 shows how the contractibility of the contour can be made explicit.

From these observations and (5), one concludes in particular that the poles of $B(\alpha_1, \alpha_2)$ can only occur at points where either α_1 or α_2 is a non-positive integer. Furthermore, $B(\alpha_1, \alpha_2) = 0$ if neither α_1 nor α_2 is a non-positive integer, but $(\alpha_1 + \alpha_2)$ is a non-positive integer. These properties of course also follow directly from (4); in fact these are precisely all the poles and zeroes of $B(\alpha_1, \alpha_2)$.

6 Contour Representation of the Function $\mathbf{B}_5$

We now view M as the real two-dimensional surface in M^c, as defined at the end of Section 2. The manifold M^c can be visualized by the complexification of Figure 3; with the edges of the pentagon taken off, M^c is now parameterized by two complex parameters that we denote as $(z_1,\ z_2)$, replacing (s, t) in (18).

Following the procedure in Section 5, let

$$\begin{aligned}&\beta_5(z_1, z_2;\, \alpha_1, \alpha_2, \alpha_3, \alpha_4, \alpha_5) = \\ &\quad = \ z_1^{\alpha_1-\alpha_2-\alpha_5} z_2^{\alpha_2-1}(1-z_1)^{\alpha_3-1}(z_1-z_2)^{\alpha_5-1}(1-z_2)^{\alpha_4-\alpha_3-\alpha_5}\ . \qquad (30)\end{aligned}$$

Then (2) can be viewed as the integral of the (locally) holomorphic 2-form $\beta_5\, dz_1 \wedge dz_2$ (with branched singularities) on M^c over the domain $\boxed{1}$ on M.

The function β_5 can be viewed as a 5-complex-parameter family of locally holomorphic functions on M^c with branched singularities at the edges of the pentagons evident in the complexification of Figure 3.

Let S be the Riemann covering sheaf of β_5 over $M^c \setminus \{\text{branch lines}\}$. We will construct an orientable closed surface in S that is the lift of a closed surface in M^c obtained by wrapping properly around the five (complex) edges of the pentagonal domain $\boxed{1}$. This will then lead to the formula (6).

A function such as β_5 is only defined on M^c, away from singularities, up to a factor $e^{2\pi i\gamma}$, i.e., by a *phase* γ which is an integer linear combination of $\alpha_1, \cdots, \alpha_5$. To lift a surface wrapping around the branch lines to the covering sheaf S, on which β_5 is a holomorphic function, we first need to understand how the phase of β_5 changes on a piece of surface as it makes a simple fold back around one branch line (see Figure 8).

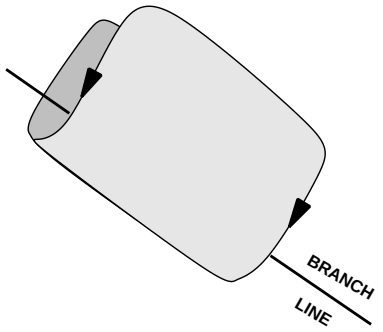

Figure 8: A surface sheet folds back around a codimension two branch line.

It is obvious that if a surface folds back around the branch line $z_2 = 0$, $z_1 = 1$, or $z_1 - z_2 = 0$, then the phase of β_5 changes by $\pm\alpha_2$, $\pm\alpha_3$, or $\pm\alpha_5$, respectively, where the sign $+$ or $-$ depends on the folding direction, i.e., whether the direction is *counterclockwise* or *clockwise*.

To see how the the phase of β_5 changes on a surface folding around the branch line A (see Figure 9), let (w_1, w_2) be the coordinates around A chosen so that A is

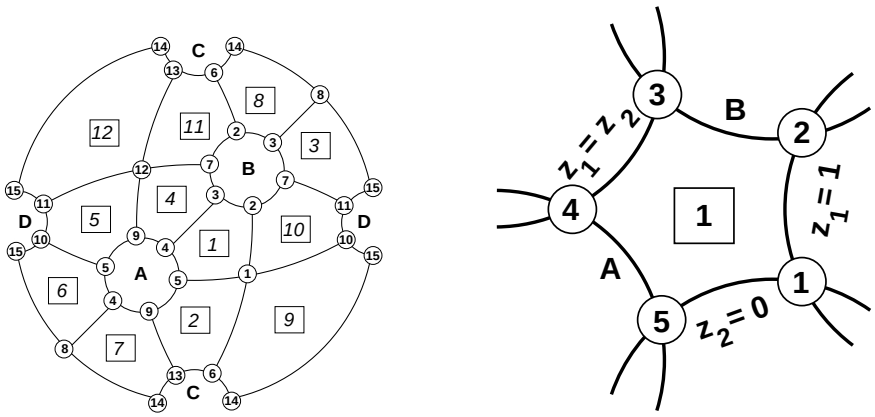

Figure 9: The pentagonal domains of the B_5 integrand, with detailed pentagonal branch structure shown for region 1.

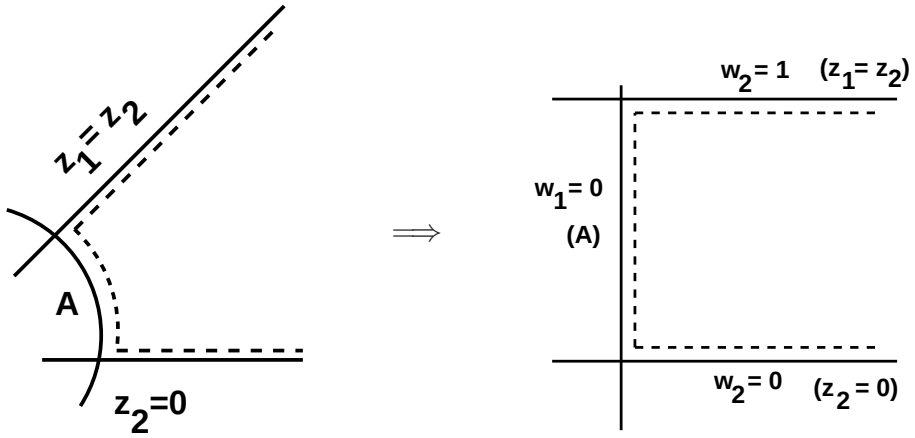

Figure 10: The coordinates around the branch line at A.

given by $w_1 = 0$, and away from A, $w_1 = z_1$, $w_2 = z_2/z_1$ (cf. [5] and Figure 10). We can then write β_5 as

$$\begin{aligned}&\beta_5(z_1, z_2;\, \alpha_1, \alpha_2, \alpha_3, \alpha_4, \alpha_5) = \\ &\quad = \; w_1^{\alpha_1 - 2} w_2^{\alpha_2 - 1} (1 - w_1)^{\alpha_3 - 1} (1 - w_2)^{\alpha_5 - 1} (1 - w_1 w_2)^{\alpha_4 - \alpha_3 - \alpha_5} \; .\end{aligned}$$

It is now easy to see that as a surface folds back around A, the phase of β_5 changes by $\pm\alpha_1$. Similarly, one can show that as a surface folds back around B, the phase of β_5 changes by $\pm\alpha_4$.

We now construct an immersed surface in M in three steps as follows:

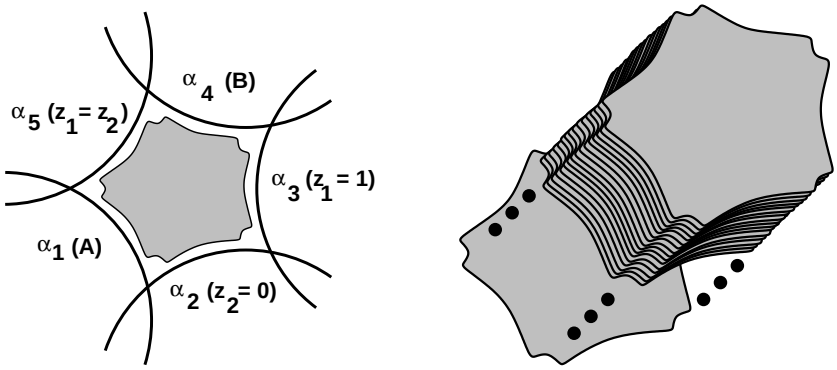

Figure 11: The pentagonal sheets in region $\boxed{1}$.

Step 1. Consider a set of 32 copies of the pentagonal sheets stacked over the region $\boxed{1}$ in Figure 9, with a small neighborhood of the five corners taken off for now. From what we have shown above, it is appropriate to label the edges of each pentagonal sheet at $A,\ z_2 = 0,\ z_1 = 1,\ B,\ z_1 - z_2 = 0$ by $\alpha_1,\ \alpha_2,\ \alpha_3,\ \alpha_4,\ \alpha_5$, respectively (see Figure 11).

We attach to each of these pentagonal sheets a *phase label*

$$p_1\alpha_1 + p_2\alpha_2 + p_3\alpha_3 + p_4\alpha_4 + p_5\alpha_5\ ,$$

where $p_j = 0$ or 1 for $j = 1, \ldots, 5$. Each pentagonal sheet is given an orientation which is same as or opposite to the original natural orientation on region $\boxed{1}$ according to whether $\sum p_j$ is even or odd.

Step 2. Two pentagonal sheets in Step 1 are joined along the edge α_j by folding around the corresponding branch line in the proper direction (see Figure 8) if and only if their phase numbers differ by α_j. It is easy to see that we end up with an immersed oriented surface in $M \setminus \{\text{branch lines}\}$ that can be lifted to S. However, this surface has *40 holes* caused by the small neighborhoods that we removed around the corners where the branch lines intersect. In Figure 12, we show a single instance of one of these holes.

Step 3. To show that one can fill in these holes, we observe that a small 3-sphere around an intersection of two branch lines, with the branch lines taken off, is homotopic to a torus and hence its fundamental group is isomorphic to the Abelian group $\mathbb{Z} \times \mathbb{Z}$. It is easy to see that the boundary of a small hole at this intersection, which lies in the surrounding 3-sphere, represents

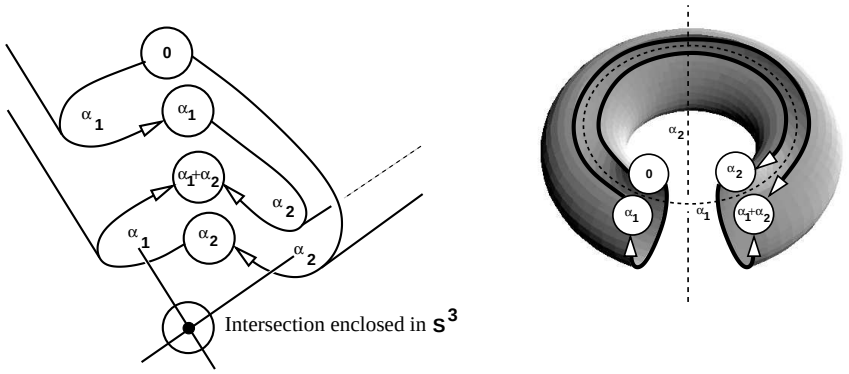

(a) (b)

Figure 12: (a) The hole at a single corner. (b) A hole-filling disk in $\mathbf{S}^3$ enclosing the intersection point of the two (complex) branch lines.

the element $(1,0)+(0,1)+(-1,0)+(0,-1) = (0,0)$ and therefore is contractible (a filled-in disk as illustrated in Figure 12(b)).

Remark: If one tries to construct such a surface directly in $\mathbb{C}^2$, then there would be a hole at a corner where three branch lines intersect, and for such holes the argument above fails.

We have therefore obtained an oriented closed surface F immersed in S, whose Euler characteristic can be easily seen to be $\chi(F) = 40 - 80 + 32 = -8$. Hence the surface F is of genus 5, i.e., a *sphere with five handles*.

Now, let

$$\epsilon(\alpha_1, \alpha_2, \alpha_3, \alpha_4, \alpha_5) = \int_F \beta_5(z_1, z_2;\ \alpha_1, \alpha_2, \alpha_3, \alpha_4, \alpha_5)\, dz_1 \wedge dz_2\ .$$

Clearly $\epsilon(\alpha_1, \alpha_2, \alpha_3, \alpha_4, \alpha_5)$ is a holomorphic function of $(\alpha_1, \alpha_2, \alpha_3, \alpha_4, \alpha_5)$ and is invariant under continuous deformations of F. As in the case of the Pochhammer contour described in Section 5, we can take the limit and calculate for suitably

restricted $(\alpha_1, \alpha_2, \alpha_3, \alpha_4, \alpha_5)$ that

$$\epsilon(\alpha_1, \alpha_2, \alpha_3, \alpha_4, \alpha_5) = \\ = (1 - e^{2\pi i \alpha_1})(1 - e^{2\pi i \alpha_2})(1 - e^{2\pi i \alpha_3})(1 - e^{2\pi i \alpha_4})(1 - e^{2\pi i \alpha_5}) \\ \cdot \iint\limits_{0<x_2<x_1<1} x_1^{\alpha_1 - \alpha_2 - \alpha_5} x_2^{\alpha_2 - 1} (1 - x_1)^{\alpha_3 - 1} (x_1 - x_2)^{\alpha_5 - 1} (1 - x_2)^{\alpha_4 - \alpha_3 - \alpha_5} \, dx_1 \, dx_2 \ .$$

This proves (6). □

Following the analogy to the B_4 Pochhammer analysis to determine further constraints on the poles and zeroes of B_5 is an interesting challenge for future work.

7 Visualizations of Connected Components and Pochhammer Contours

The analysis of the B_5 function in the previous sections has been based entirely on algebraic manipulations and line drawings sketching the essential features of the geometry. This section is motivated by the observation that, since there are algebraic constructions for every geometric concept, we can go one step further and show precise images of each construction, helping the reader to develop a quantitative as well as a qualitative understanding of the framework we have developed. We establish the basic context with some examples based on the Euler Beta function, and then proceed to show some of the remarkable manifolds that occur in the B_5 analysis.

7.1 B_4 Connected Components Embedded in a Veronese Surface

The Euler Beta function itself can be analyzed using cross-ratio coordinates. We begin with the two cross-ratio variables, x_1 and x_2, obeying the apparently uninteresting constraint

$$x_1 = 1 - x_2 \ .$$

However, when we put this into homogeneous coordinates $\{x_0, x_1, x_2\}$, the constraint becomes $x_0 = x_1 + x_2$, and we can solve these equations independently in the three component regions, written as three intervals in inhomogeneous coordinates as $A = [0, 1]$, $B = [1, \infty]$, and $C = [-\infty, 0]$. Noting that the space we are

now dealing with is *not* $\mathbb{C}$ or $\mathbb{C}\mathbf{P}^1$, but the real part of the $\mathbb{C}\mathbf{P}^2$ *cross-ratio-space*, we can parameterize each interval in homogeneous $\mathbb{R}\mathbf{P}^2$ coordinates as follows:

$$\begin{aligned} A(t): &\quad [1,\, t,\, (1-t)] \\ B(t): &\quad [(1-t),\, 1,\, -t] \\ C(t): &\quad [-t,\, (1-t),\, -1]\ . \end{aligned} \tag{31}$$

We see that region A solves $1 = x_1 + x_2$ with $x_1 = t$, B solves $1 = x_1 + x_2$ with $x_1 = 1/(1-t)$ when all is multiplied by $(1-t)$, and C solves $1 = x_1 + x_2$ with $x_1 = (t-1)/t$ when all is multiplied by t. The interpolating functions in the three regions obviously correspond to the three B_4 component regions introduced initially in Figure (1), and they interpolate between the points represented in the Riemann-sphere depiction of Figure 13:

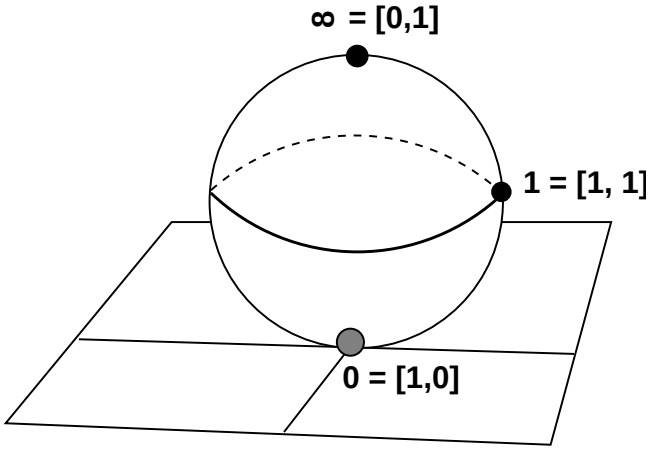

Figure 13: The full base space of the B_4 branched covering, showing the three regions corresponding to the three intervals $(0,1)$, $(1,\infty)$, and $(-\infty,0)$ on the real projective line.

				$\mathbb{R}\mathbf{P}^2$ homog		$\mathbb{C}\mathbf{P}^1(z_0,z_1)$		$\mathbb{C}$ inhomog (z_1/z_0)
p_1	$=$	$A(0)$	$=$	$[1,0,1]$	$\approx$	$z=[1,0]$	$\approx$	$x=0$
p_2	$=$	$B(0)$	$=$	$[1,1,0]$	$\approx$	$z=[1,1]$	$\approx$	$x=1$
p_3	$=$	$C(0)$	$=$	$[0,1,-1]$	$\approx$	$z=[0,1]$	$\approx$	$x=\pm\infty$.

But there is a small problem: if we follow the coordinate interpolations carefully, they only work projectively; the actual interpolations close on one another

only if we include the negative, projectively-equivalent points $\bar{p}_i = -p_i$, for a total of 6 points and six linear paths, rather than three. Thus, the projective coordinates for the three components $A,\ B,\ C$ can be plotted either as a connected hexagon in $\mathbb{R}^3$, the embedding space of the homogeneous $\mathbb{R}\mathbf{P}^2$ coordinates, or as a more visually consistent projection onto a constant-radius $\mathbf{S}^2$, the double-cover of $\mathbb{R}\mathbf{P}^2$, as shown in Figure 14(a).

To actually achieve the desired end result of a visualization of the B_4 cross-ratio coordinates in a logical embedding, we must find a quadratic map that removes the distinction between the positive and negative versions of the same projective coordinates and maps $\mathbf{S}^2$ explicitly to $\mathbb{R}\mathbf{P}^2$. This is achieved classically by the Veronese surface (see, e.g., the traditional embedding of $\mathbb{R}\mathbf{P}^2$ given in the appendix of Hilbert and Cohn-Vossen, [7]):

$$\begin{array}{ccc} w_1 = \sqrt{2}x_0x_1 & w_2 = \sqrt{2}x_0x_2 & w_3 = \sqrt{2}x_1x_2 \\ w_4 = (x_0)^2 & w_5 = (x_1)^2 & w_6 = (x_2)^2 \end{array} \tag{32}$$

where the spherical constraint ${x_0}^2 + {x_1}^2 + {x_2}^2 = 1$ implies the standard Veronese surface constraint $\sum(w_i)^2 = \left(\sum(x_k)^2\right)^2 = 1$. In Figures 14(b) and (c), we see the exact paths of the three component integrals of the Euler Beta function as they are embedded in alternate projections of $\mathbb{R}\mathbf{P}^2$ (the real part of $\mathbb{C}\mathbf{P}^2$) to 3D. This is equivalent mathematically, and yet a significantly contrasting viewpoint, to the conventional $\mathbb{C}\mathbf{P}^1$ alternative indicated in Figure 13.

7.2 Visualizing the B_4 Pochhammer Contour

We now illustrate explicitly the geometry of the Pochhammer contour for the Euler Beta function. Starting from (29), we choose a pair of small relatively prime rational exponents $(\alpha_1,\ \alpha_2)$, and project the 4D plot of $w = \beta(z; \alpha_1, \alpha_2)$ to 3D, with the horizontal plane parameterized by $x = \mathrm{Re}(z)$, $y = \mathrm{Im}(z)$, and the vertical axis given by $\mathrm{Re}(w)$. Figure 15(a) shows a small region of the branched Riemann cover of the complex plane punctured at $z = 0$ and $z = 1$, and Figure 15(b) shows the precise path in this branched cover of the Pochhammer "commutator" contour sketched in Figure 6, but now as an actual embedding in $\mathbb{C}^2$ (technically $\mathbb{R}^4$ projected to $\mathbb{R}^3$). Figure 15(c) combines the two views to show the Pochhammer contour in its geometric context on the Riemann surface.

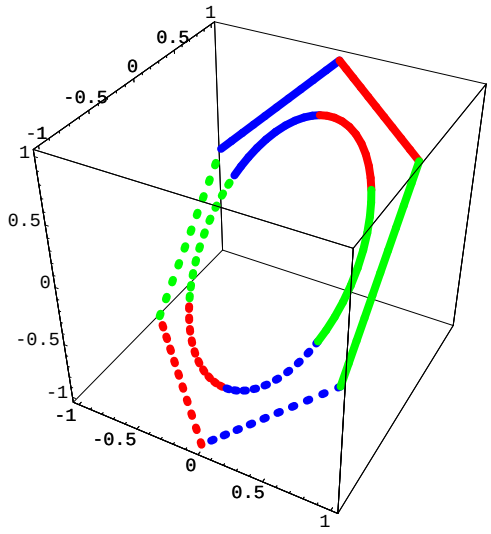

(a)

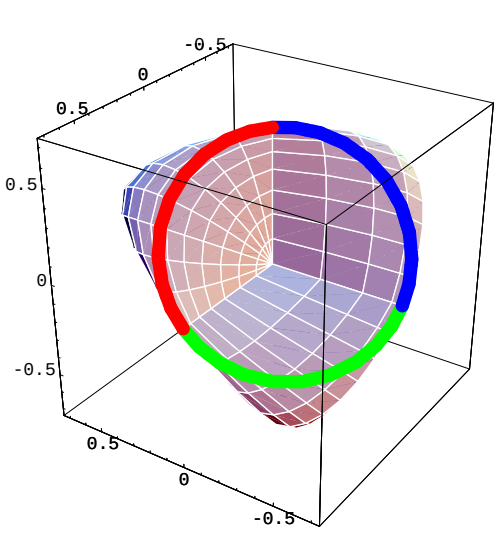

(b)

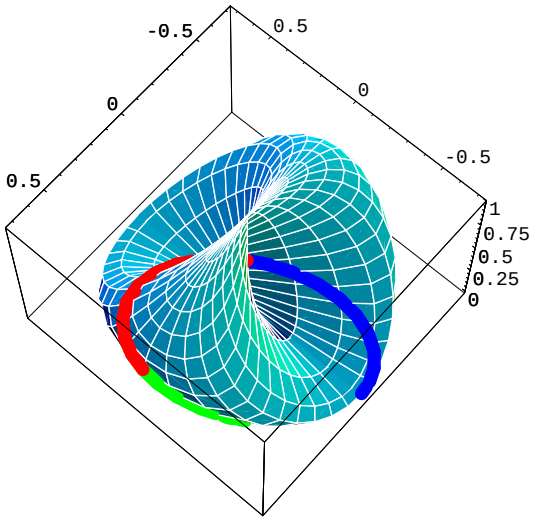

(c)

Figure 14: (a) The double cover of B_4 branched covering, showing the linear interpolations among the points $p_1 = (1, 0, 1), \bar{p}_1 = (-1, 0, -1), p_2 = (1, 1, 0), \bar{p}_2 = (-1, -1, 0), p_3 = (0, 1, -1), \bar{p}_3 = (0, -1, 1)$ and their projections to $\mathbf{S}^2$. (b) The Veronese map, projected to the Steiner Roman Surface, (w_1, w_2, w_3). (c) Projection onto the crosscap, (w_1, w_2, w_6).

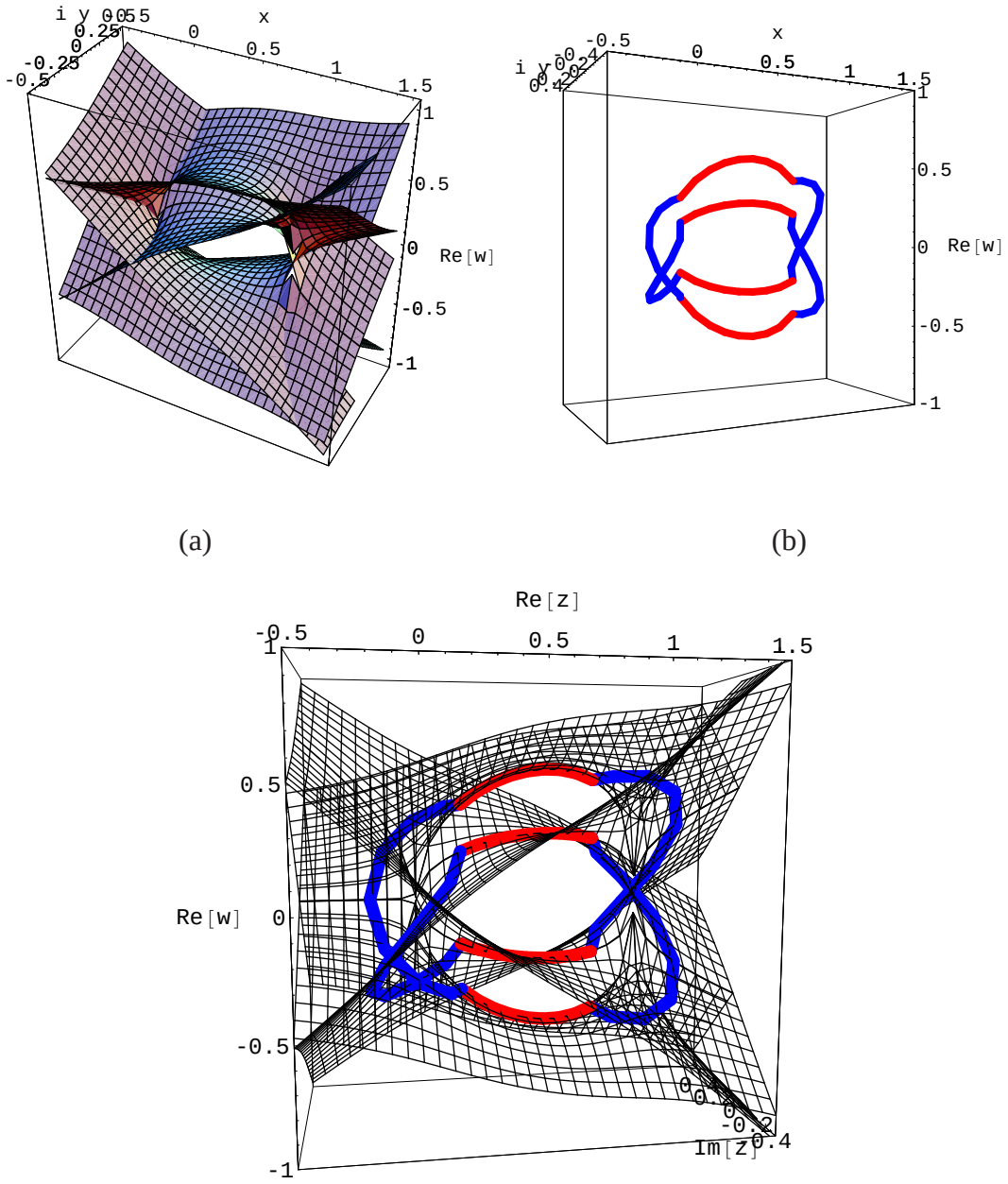

Figure 15: (a) A representative Riemann surface derived from the integrand of the Euler Beta function with suitable rational values of (α_1, α_2). (b) The actual geometry of the Pochhammer contour traced on the representative Riemann surface. The path on the Riemann surface is a "commutator," encircling each branch point once in each direction; comparing to Figure 6, the four end loops shrink to points as $r \to 0^+$. (c) Combined plot.

7.3 B_5: Components of the 5-Point Cross-Ratios

The four single lines joined by infinitesimal loops shown in Figures 6 and 15 represent the four distinct *phases* of the B_4 Pochhammer integration path. For B_5, the analog of one of these lines is a pentagonal surface, and the set of four lines representing integration domain of B_4 with distinct phases is replaced in B_5 by 32 pentagons with distinct phases. Just as the three lines in Figure 13 or Figure 14 describe the three *components* of B_4 that followed from solving the cross-ratio constraint, the twelve components of B_5 can be studied using parametric solutions of its own cross-ratio constraint system: re-indexing for convenience using $(z_1, z_2, z_3, z_4, x_5) \equiv (u_{12}, u_{13}, u_{23}, u_{24}, u_{34})$, the B_5 cross-ratio system becomes:

$$\begin{aligned} z_1 &= 1 - z_3 z_4 \\ z_2 &= 1 - z_4 z_5 \\ z_3 &= 1 - z_5 z_1 \\ z_4 &= 1 - z_1 z_2 \\ z_5 &= 1 - z_2 z_3 \ . \end{aligned} \tag{33}$$

Any pentagon can be represented algebraically by picking two of the five z_i's as independent, and plotting any of the dependent variables found by solving the constraints in formula (33) on the third axis. The typical result, shown in Figure 16, is an algebraic 2-manifold embedded in $\mathbb{R}^5$ showing the integration region over the variety given by (33). Projected from a horizontal direction, the pentagon of Figure 16(a) becomes a square region, whereas when projected from the vertical direction, it becomes a triangular region, corresponding to formula (2).

To create an image of the twelve B_5 components, we now use the constraints (33) and proceed through the same arguments that we used for B_4: We solve the constraints in a family of homogeneous $\mathbb{R}\mathbf{P}^5$ coordinates based on choosing non-singular parameterizations of $(z_0, z_1, z_2, z_3, z_4, z_5)$, and find that the natural connectivity actually gives us initially the 24-pentagon double cover analogous to the six B_4 curves shown in Figure 14(a). Figure 17 is the schematic analog of Figure 13 for B_4, showing the topological diagram of the surface, which we can verify is non-orientable with 15 vertices, 30 edges, and 12 pentagonal faces, giving the advertised Euler characteristic $\chi = -3$, a sphere with five crosscaps. However, we can also see traced on this surface the family of complex lines that form the symmetrized base of the branched cover enabled by the blow-ups: there are 10 separate interlocking triangles, each denoting the (circular) real line of a $\mathbb{C}\mathbf{P}^1$ corresponding precisely to the B_4 diagram of Figure 13 or 14(b); treating

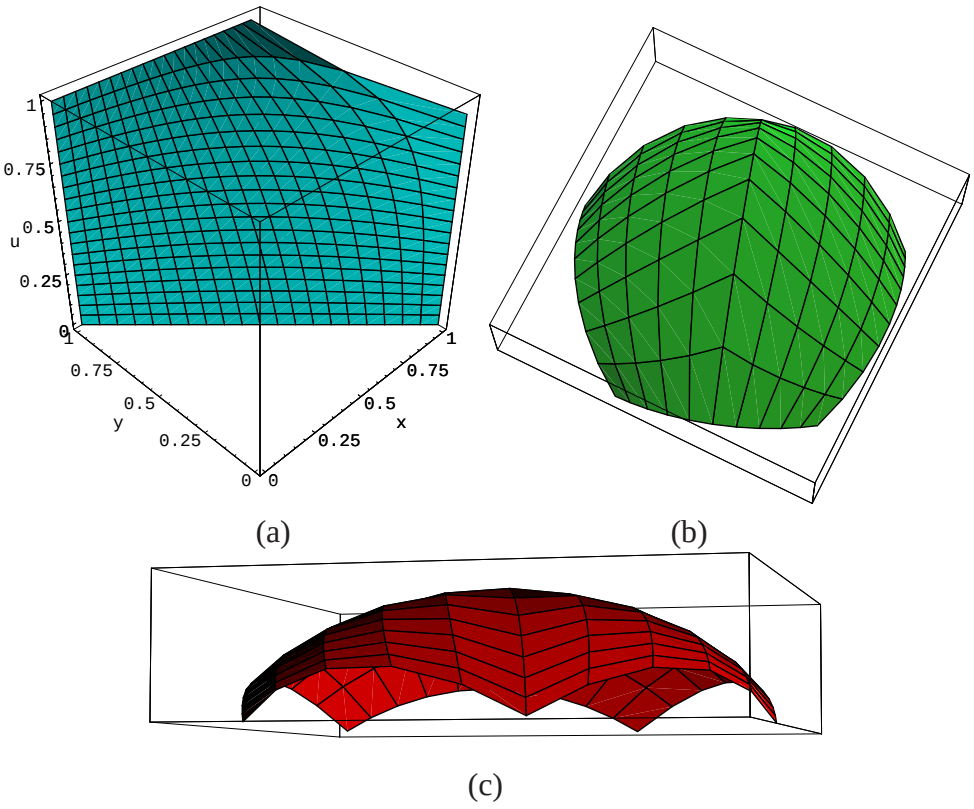

Figure 16: (a) Plotting the B_5 variables $(x, (1-x)/(1-xy), y)$, showing how the "blown-up" pentagonal manifold arises naturally in the cross-ratio manifold. (b) Completely regular version of the pentagonal, normalized to $\mathbf{S}^5$ and projected, corresponding to the variables of Figure 4. (c) Side view of (b).

these schematically as filled-in triangles, we get the image in Figure 18, where the boundaries of the 10 triangles taken five at a time bound the 12 pentagons. The corresponding 12-pentagon figure can be thought of as shown in Figure 17, where the boundaries of the connected components (corresponding to $-\alpha_1 - \alpha_2$ for B_4) are linear combinations of the B_5 α_i's. In particular, the face labeled "12" corresponds to a B_5 function with a set of exponents that is distinct from the values $(\alpha_1, \alpha_2, \alpha_3, \alpha_4, \alpha_5)$ used in (2), although they are closely related. One can show with suitable variable changes that the exponents corresponding to the

primed branch lines (analogous to the exponent at infinity for B_4) are

$$\begin{aligned} \alpha'_1 &= 1+\alpha_1-\alpha_2-\alpha_5 \\ \alpha'_2 &= 1+\alpha_2-\alpha_3-\alpha_1 \\ \alpha'_3 &= 1+\alpha_3-\alpha_4-\alpha_2 \\ \alpha'_4 &= 1+\alpha_4-\alpha_5-\alpha_3 \\ \alpha'_5 &= 1+\alpha_5-\alpha_1-\alpha_4\ . \end{aligned} \tag{34}$$

The solutions of the constraints are continuous only in the double cover, so we will work first in an unnormalized $\mathbb{R}\mathbf{P}^5$ to produce the analogs of the six end points and six straight interpolating edges that we showed in Figure 14(a) for B_4. This equivalent set of vertices is the set of 10 hexagons representing the double cover of the $\mathbb{C}\mathbf{P}^1$ branch lines denoted by $(\alpha_1,\ldots,\alpha'_1,\ldots)$, as shown in Figure 19. These have the following vertex assignments in the double cover:

line α_1 :	$(1,5,10,-1,-5,-10)$	line α'_1 :	$(10,15,11,-10,-15,-11)$
line α_2 :	$(2,1,6,-2,-1,-6)$	line α'_2 :	$(6,13,14,-6,-13,-14)$
line α_3 :	$(3,2,7,-3,-2,-7)$	line α'_3 :	$(7,11,12,-7,-11,-12)$
line α_4 :	$(4,3,8,-4,-3,-8)$	line α'_4 :	$(8,14,15,-8,-14,-15)$
line α_5 :	$(5,4,9,-5,-4,-9)$	line α'_5 :	$(9,12,13,-9,-12,-13)$.

Each region is bounded by a linear interpolation connecting the (doubled) vertex set, as noted earlier.

Figure 20 shows the actual doubled geometry, both as straight lines in $\mathbb{R}^6$, and as curves in the sphere $\mathbf{S}^5$ (projected to 3D).

Fully Symmetric Vertex Choice. If all we were interested in was the descriptive topology of the B_5 five-crosscap base manifold, any set of vertices with the proper connectivity would be sufficient. However, our dual purpose is to understand not only the topology, but also any unique geometric features or symmetries that might characterize this manifold, leading to embeddings whose graphical depictions might be especially informative.

We have therefore pursued the search for special embeddings one step further, and computed an orthonormalized set of vertices along with the corresponding surface embedding that allows all pentagons to be expressed as rigid transformations of one another derived from the operations of the discrete symmetry operators of Section 4.

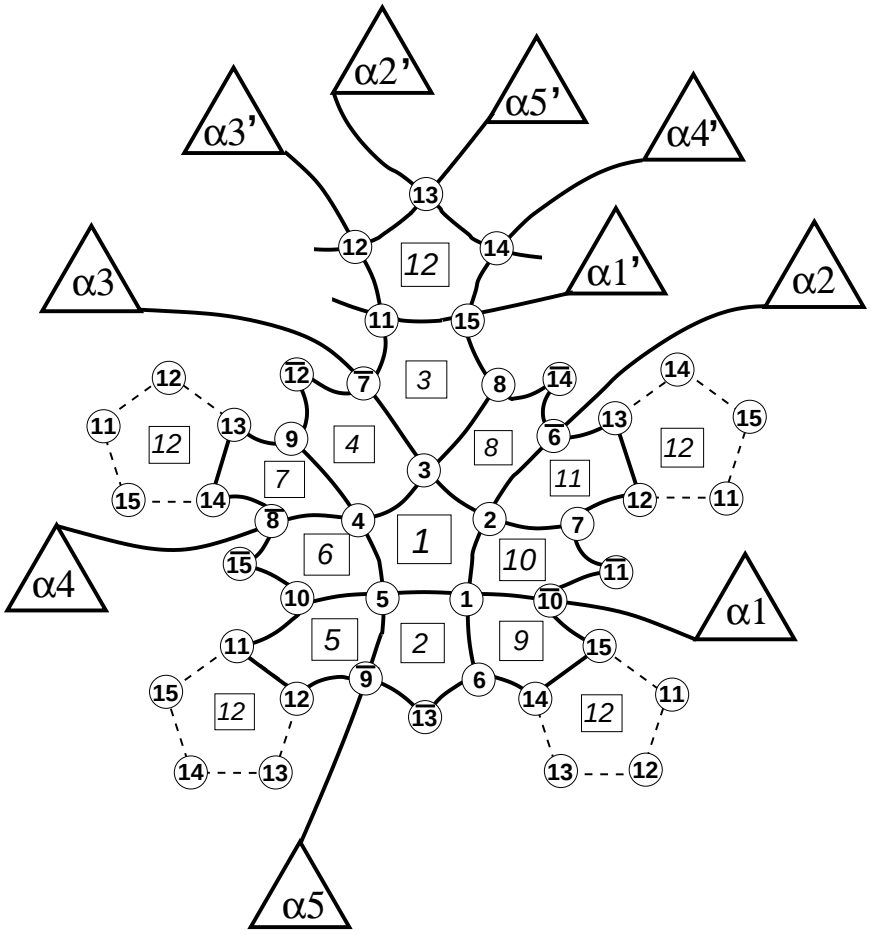

Figure 17: The diagram of how the 12 pentagonal pieces of surface join together to form a closed surface in $\mathbb{R}\mathbf{P}^5$. Circles mark the 15 vertices, and squares mark the images of the corresponding regions in Figure 2. Triangles label the exponent of each of the branch lines delineating the connected components. (See (34).)

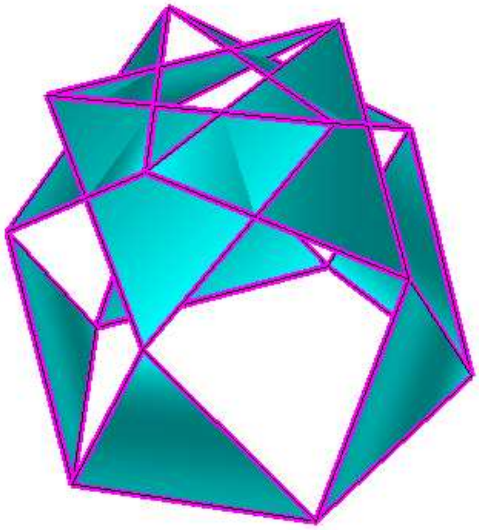

Figure 18: These 10 filled triangles represent the single cover of the 10 $\mathbb{C}\mathbf{P}^1$ branch surfaces of the B_5 integrand Riemann manifold, The straight edges taken 5 at a time bound the 12 pentagons.

The next step is to use the matrix P defined by (26). Such a P can be found from standard linear algebra methods; we will not write P explicitly because its entries are not rational numbers and are very lengthy.

Let

$$\begin{aligned} F^{\pm}(s,t) &= P \cdot \tilde{f}^{\pm}(s,t) \\ &= \pm \frac{P \cdot f_i}{\sqrt{f_i^t \cdot Q \cdot f_i}} \end{aligned}$$

We then get the transformation $P \cdot \widetilde{M}$ of the surface $\widetilde{M}$. Notice that $P \cdot \widetilde{M}$ is in $\mathbf{S}^5$ and is invariant under

$$\gamma = P \cdot g \cdot P^{-1}$$

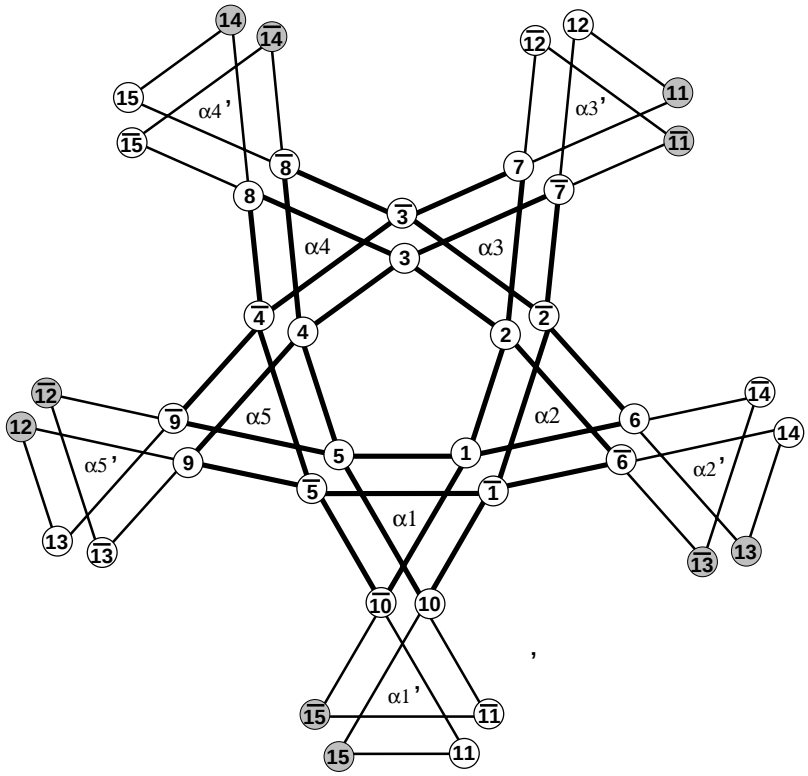

Figure 19: An explicit graph of the double covering of the cross-ratio variable space, showing each vertex and each of the 10 hexagons corresponding individually to a double-covered $\mathbb{C}\mathbf{P}^1$ branch line, and also to the hexagon in Figure 14. It is easy to see how Figure 18 emerges as the single-cover after reducing each hexagon to a triangle.

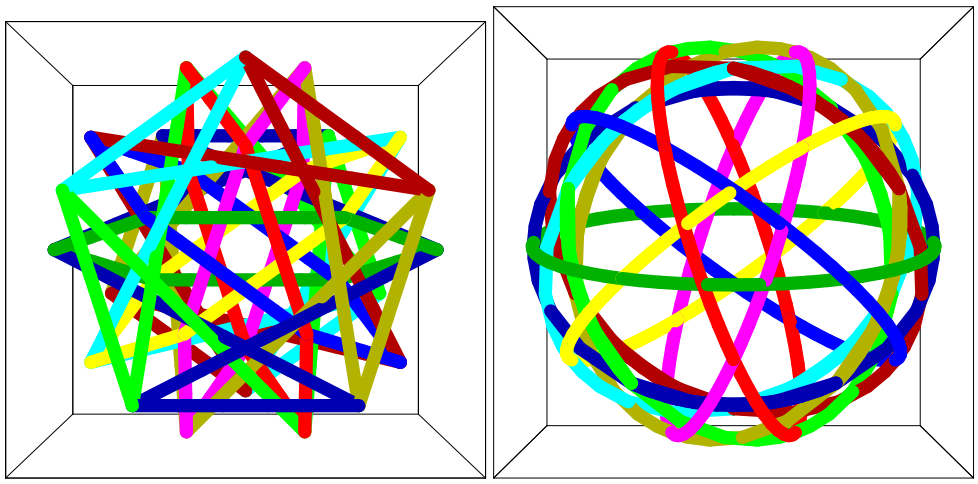

(a) (b)

Figure 20: (a) Projection from homogeneous $\mathbb{R}^6$ coordinates of all the $2 \times 30 = 60$ straight edges giving edges of pentagons (or real lines of the $\mathbb{C}\mathbf{P}^1$ branches) in the double cover, the analogs of the six *end points* in Figure 14(a). (b) Normalization to $\mathbf{S}^5$, analogous to the same six points on $\mathbf{S}^2$ in 14(a).

for $g \in \widetilde{G}$; the γ's are now the orthogonal matrices forming a subgroup of order 240 in $\mathbf{O}(6)$.

We pick the following 24 elements from this group:

$$\gamma_1^{\pm} = \pm\text{Identity} \qquad \gamma_2^{\pm} = \pm P \cdot \begin{bmatrix} 1 & 0 & 0 & -1 & 0 & 0 \\ 2 & 0 & -1 & -1 & 0 & -1 \\ 0 & 0 & 0 & -1 & 0 & 0 \\ 2 & -1 & 0 & -1 & -1 & 0 \\ 0 & 0 & 0 & 0 & 0 & 1 \\ 0 & 1 & 0 & 0 & 0 & 0 \end{bmatrix} \cdot P^{-1}$$

$$\gamma_3^{\pm} = \pm P \cdot \begin{bmatrix} -1 & 0 & 0 & 1 & 0 & 1 \\ 0 & 0 & 0 & 0 & 0 & 1 \\ 2 & -1 & -1 & 0 & -1 & 0 \\ 0 & 0 & 0 & 1 & 0 & 0 \\ -2 & 0 & 1 & 1 & 0 & 1 \\ -2 & 1 & 0 & 1 & 0 & 1 \end{bmatrix} \cdot P^{-1} \qquad \gamma_4^{\pm} = \pm P \cdot \begin{bmatrix} 1 & 0 & 0 & 0 & 0 & -1 \\ 2 & -1 & 0 & -1 & 0 & -1 \\ 0 & 0 & 1 & 0 & 0 & 0 \\ 0 & 0 & 0 & 1 & 0 & 0 \\ 2 & 0 & -1 & 0 & -1 & -1 \\ 0 & 0 & 0 & 0 & 0 & -1 \end{bmatrix} \cdot P^{-1}$$

$$\gamma_5^{\pm} = \pm P \cdot \begin{bmatrix} -1 & 1 & 0 & 1 & 0 & 0 \\ -2 & 1 & 0 & 1 & 0 & 1 \\ -2 & 1 & 0 & 1 & 1 & 0 \\ 0 & 0 & 0 & 1 & 0 & 0 \\ 2 & 0 & -1 & 0 & -1 & -1 \\ 0 & 1 & 0 & 0 & 0 & 0 \end{bmatrix} \cdot P^{-1} \qquad \gamma_6^{\pm} = \pm P \cdot \begin{bmatrix} 1 & -1 & 0 & 0 & 0 & 0 \\ 0 & -1 & 0 & 0 & 0 & 0 \\ 2 & -1 & -1 & 0 & -1 & 0 \\ 0 & 0 & 0 & 1 & 0 & 0 \\ 0 & 0 & 0 & 0 & 1 & 0 \\ 2 & -1 & 0 & -1 & 0 & -1 \end{bmatrix} \cdot P^{-1}$$

$$\gamma_7^{\pm} = \pm P \cdot \begin{bmatrix} -1 & 0 & 1 & 0 & 0 & 1 \\ -2 & 0 & 1 & 1 & 0 & 1 \\ 0 & 0 & 1 & 0 & 0 & 0 \\ 2 & -1 & 0 & -1 & -1 & 0 \\ 0 & 0 & 0 & 0 & 0 & 1 \\ -2 & 0 & 1 & 0 & 1 & 1 \end{bmatrix} \cdot P^{-1} \qquad \gamma_8^{\pm} = \pm P \cdot \begin{bmatrix} 1 & 0 & 0 & 0 & -1 & 0 \\ 0 & 1 & 0 & 0 & 0 & 0 \\ 0 & 0 & 1 & 0 & 0 & 0 \\ 2 & -1 & 0 & -1 & -1 & 0 \\ 0 & 0 & 0 & 0 & -1 & 0 \\ 2 & 0 & -1 & 0 & -1 & -1 \end{bmatrix} \cdot P^{-1}$$

$$\gamma_9^{\pm} = \pm P \cdot \begin{bmatrix} -1 & 1 & 0 & 0 & 1 & 0 \\ 0 & 0 & 0 & 0 & 1 & 0 \\ -2 & 1 & 0 & 1 & 1 & 0 \\ -2 & 1 & 1 & 0 & 1 & 0 \\ 0 & 1 & 0 & 0 & 0 & 0 \\ 2 & 0 & -1 & -1 & 0 & -1 \end{bmatrix} \cdot P^{-1} \qquad \gamma_{10}^{\pm} = \pm P \cdot \begin{bmatrix} 1 & 0 & -1 & 0 & 0 & 0 \\ 0 & 0 & 0 & 0 & 0 & 1 \\ 2 & -1 & -1 & 0 & -1 & 0 \\ 0 & 0 & -1 & 0 & 0 & 0 \\ 2 & 0 & -1 & -1 & 0 & -1 \\ 0 & 0 & 0 & 0 & 1 & 0 \end{bmatrix} \cdot P^{-1}$$

$$\gamma_{11}^{\pm} = \pm P \cdot \begin{bmatrix} -1 & 0 & 1 & 0 & 1 & 0 \\ 2 & -1 & 0 & -1 & 0 & -1 \\ 0 & 0 & 1 & 0 & 0 & 0 \\ -2 & 1 & 1 & 0 & 1 & 0 \\ -2 & 0 & 1 & 0 & 1 & 1 \\ 0 & 0 & 0 & 0 & 1 & 0 \end{bmatrix} \cdot P^{-1} \qquad \gamma_{12}^{\pm} = \pm P \cdot \begin{bmatrix} 3 & -1 & -1 & -1 & -1 & -1 \\ 2 & 0 & -1 & 0 & -1 & -1 \\ 2 & -1 & -1 & 0 & -1 & 0 \\ 2 & -1 & 0 & -1 & -1 & 0 \\ 2 & -1 & 0 & -1 & 0 & -1 \\ 2 & 0 & -1 & -1 & 0 & -1 \end{bmatrix} \cdot P^{-1} \tag{35}$$

Then, the entire 5-crosscap surface or its genus-5 double cover can be constructed piece by piece starting from a single pentagon F_1 and then transforming by $\gamma_i^{\pm}$.

In Figure 21, we plot a pair of projections of the 24 surface patches $\gamma_i^{\pm} \cdot F_1(s,t)$ from $\mathbf{S}^5$ in $\mathbb{R}^6$ to $\mathbb{R}^3$. These are global solutions of the 5-point cross-ratio constraints with diametrically opposite copies of each of the 12 pentagons forming the genus 5 double cover.

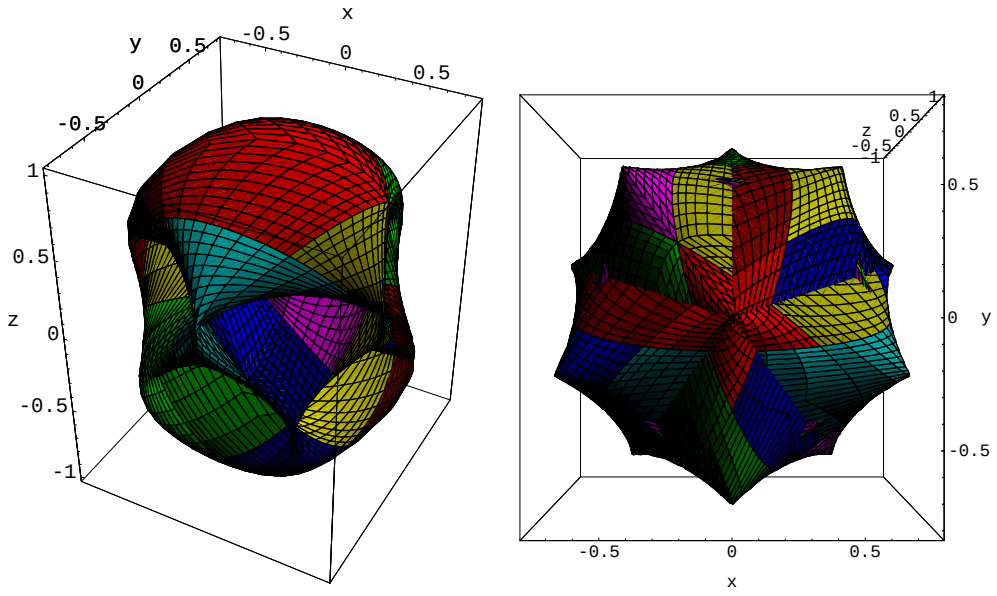

Figure 21: Projections from $\mathbb{R}\mathbf{P}^5$ to $\mathbf{S}^5$ of the double cover of the 12 blown-up pentagons forming a 5-crosscap dodecahedron. The first projection emphasizes the smooth nature of the overall surface, while the second projection emphasizes the pentagonal structure.

$\mathbf{B}_5$ Veronese Map. These vertices and the polygonal faces of the dodecahedron inscribed on the B_5's "real" integration manifold, a sphere with five crosscaps, can be compactly embedded for visualization purposes using a quadratic form that is a straightforward generalization of the Veronese surface parameterization. Given the homogeneous $\mathbb{R}\mathbf{P}^5$ variables $r = (r_0,\, r_1,\, r_2,\, r_3,\, r_4,\, r_5)$ above, we can construct an $\mathbb{R}^{21}$ embedding as

$$\begin{array}{lllllllll}
w_1 &=& cr_0r_1 & w_2 &=& cr_0r_2 & w_3 &=& cr_0r_3 \\
w_4 &=& cr_0r_4 & w_5 &=& cr_0r_5 & w_6 &=& cr_1r_2 \\
w_7 &=& cr_1r_3 & w_8 &=& cr_1r_4 & w_9 &=& cr_1r_5 \\
w_{10} &=& cr_2r_3 & w_{11} &=& cr_2r_4 & w_{12} &=& cr_2r_5 \\
w_{13} &=& cr_3r_4 & w_{14} &=& cr_3r_5 & w_{15} &=& cr_4r_5 \\
w_{16} &=& (r_0)^2 & w_{17} &=& (r_1)^2 & w_{18} &=& (r_2)^2 \\
w_{19} &=& (r_3)^2 & w_{20} &=& (r_4)^2 & w_{21} &=& (r_5)^2\,.
\end{array}$$

This map is constructed to lie on the sphere $\sum_i (w_i)^2 = 1$ when $c = \sqrt{2}$ and the homogeneous coordinates are normalized to obey $\sum_k (r_k)^2 = 1$. Note that

the analog of the Steiner Roman Surface immersion projecting $\mathbb{R}\mathbf{P}^2$ into $\mathbb{R}^3$ is achieved by selecting the variables $(w_1, \ldots, w_{15})$ mapping $\mathbb{R}\mathbf{P}^5$ into $\mathbb{R}^{15}$.

An alternative, but less symmetric, $\mathbb{R}^{18}$ embedding is

$$\begin{array}{lllllllll}
w_1 &=& 2r_0r_1 & w_2 &=& \sqrt{2}r_0r_2 & w_3 &=& \sqrt{2}r_0r_3 \\
w_4 &=& \sqrt{2}r_0r_4 & w_5 &=& \sqrt{2}r_0r_5 & w_6 &=& \sqrt{2}r_1r_2 \\
w_7 &=& \sqrt{2}r_1r_3 & w_8 &=& \sqrt{2}r_1r_4 & w_9 &=& \sqrt{2}r_1r_5 \\
w_{10} &=& 2r_2r_3 & w_{11} &=& \sqrt{2}r_2r_4 & w_{12} &=& \sqrt{2}r_2r_5 \\
w_{13} &=& \sqrt{2}r_3r_4 & w_{14} &=& \sqrt{2}r_3r_5 & w_{15} &=& 2r_4r_5 \\
w_{16} &=& (r_0)^2 - (r_1)^2 & w_{17} &=& (r_2)^2 - (r_3)^2 & w_{18} &=& (r_4)^2 - (r_5)^2 \,,
\end{array}$$

which also lies on the sphere $\sum_i (w_i)^2 = 1$ when $\sum_k (r_k)^2 = 1$.

Projections of the (non-double-covered) 5-crosscap surface can at last be drawn using these quadratic maps, and typical results are shown in Figure 22.

7.4 The B_5 Pochhammer Contour

Within the domain of a *single pentagon*, we can now finally begin to piece together a picture of the global topology of the B_5 Pochhammer contour. This manifold can be drawn explicitly in various ways by joining together the sets of commutators that eventually return to the same phase, forming the closed surface; Figure 23 illustrates a single commutator element. Figure 24 shows the schematic diagram of the full set of commutators as they return cyclically to the home phase; this diagram can be unfolded in various ways to show the overall structure, as illustrated in Figures 25 and 26.

Finally, the explicit algebraic form of the Pochhammer can be embedded directly in the Riemann manifold of $\beta_5(x, y; \alpha_1, \ldots, \alpha_5)$, following the fashion of Figure 15 to yield the surfaces shown in Figure 27. This image shows one-fifth of the Pochhammer contour covering a set of eight of the 32 total surfaces; sewing together all the corresponding copies yields the entire surface.

8 Remarks on the General Case

The affine variety defined by the N-point cross-ratio constraints (11) is of dimension $(N-3)$ and has a natural decomposition into $(N-1)!/2$ smooth components delineated by the varieties $u_{ij} = 0$. The N-point function B_N is initially defined as an integral of an $(N-3)$-form over a *single one* of these components. Each

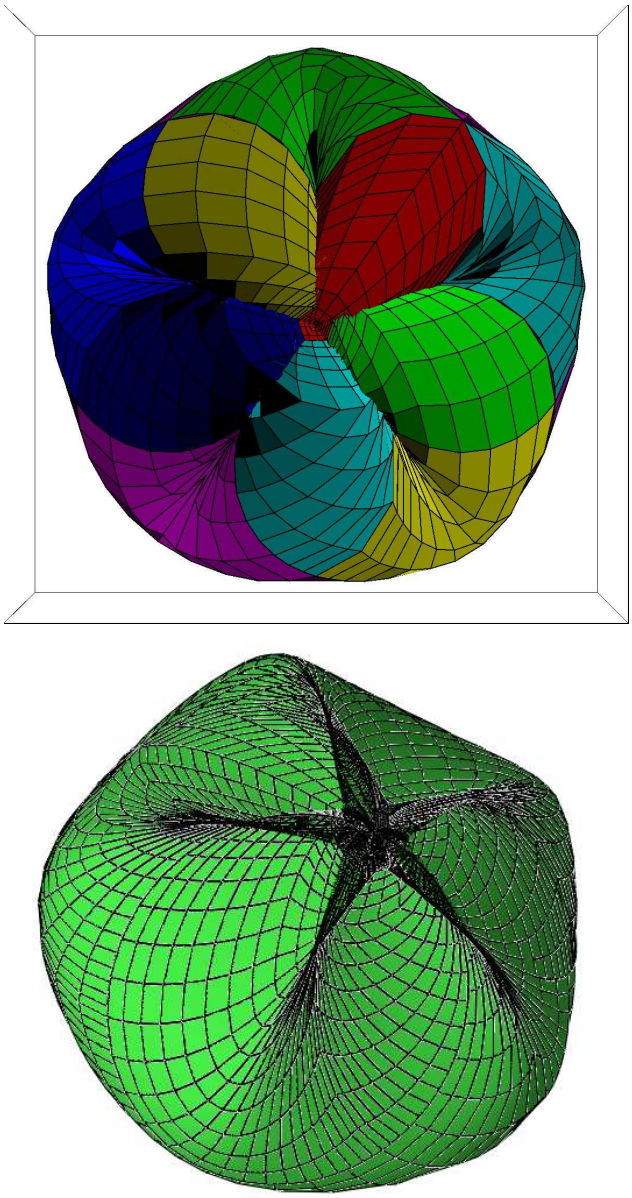

Figure 22: Projections of the 5-crosscap surface embedded in $\mathbb{R}^{21}$ using the quadratic map. Above: the (1,2,5) projection color coded by pentagon. Below: the (1,2,16) projection with shaded surface and grid. These are roughly the analogs of the projections of the circle embedded in the projective plane in Figure 14.

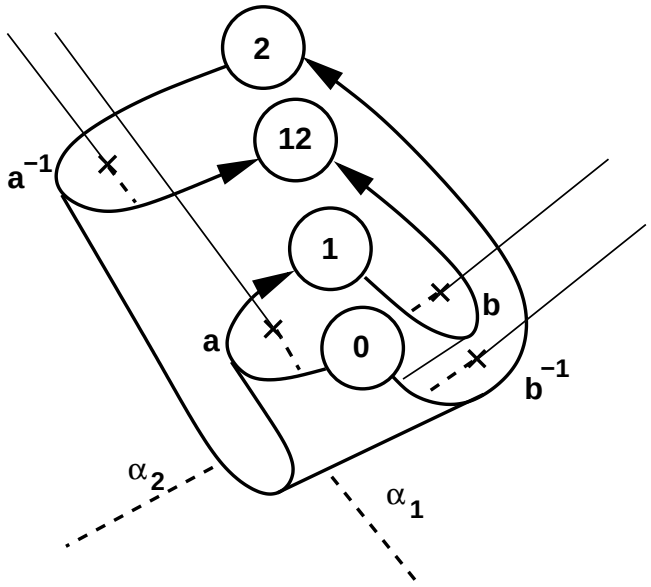

Figure 23: The B_5 "commutator" $aba^{-1}b^{-1}$ bounding a patch that covers one-fifth of each of four different phases, which for the example branch lines with exponents α_1 and α_2, are labeled as $\{0,\ 1,\ 12,\ 2\}$.

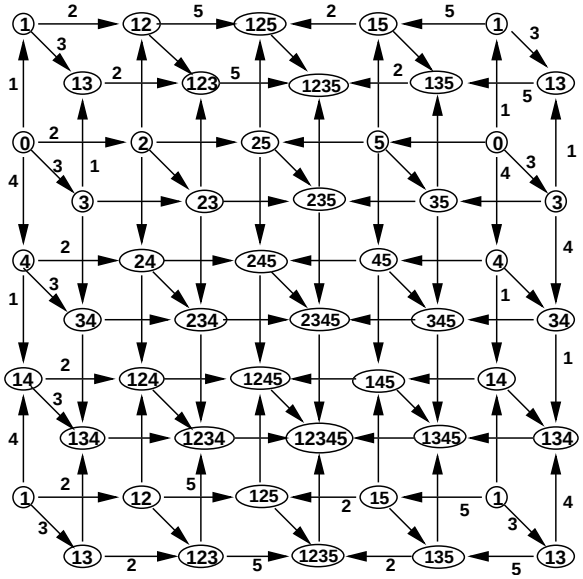

Figure 24: The commutator diagram of the B_5 Pochhammer surface.

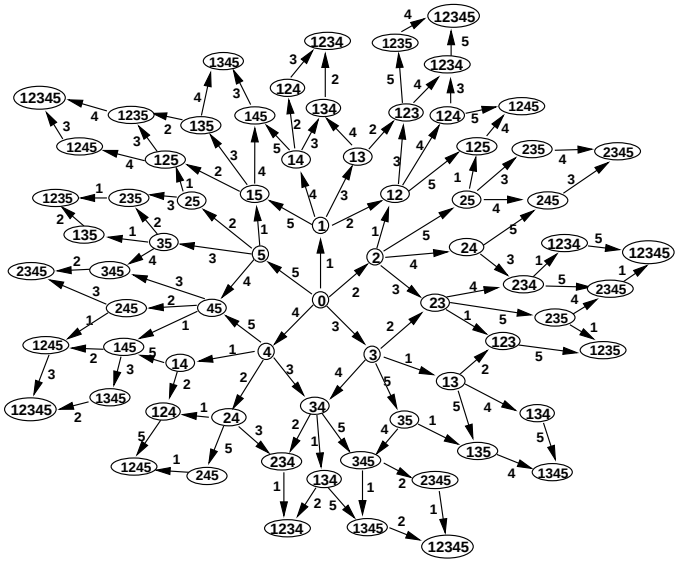

Figure 25: The analog of the Pochhammer surface for B_5 is a 32-fold cover of a single pentagon, joining each of the 2^5 possible combinations of the 5 phases $\{\alpha_1, \ldots, \alpha_5\}$. This surface can be constructed from (32/4)*5=40 individual commutator patches.

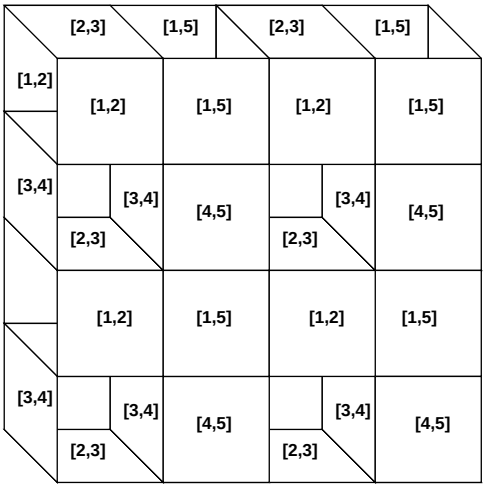

Figure 26: A global picture of the B_5 Pochhammer surface as an unrolled, thickened torus with four punctures, showing more clearly the origin of its genus 5 structure.

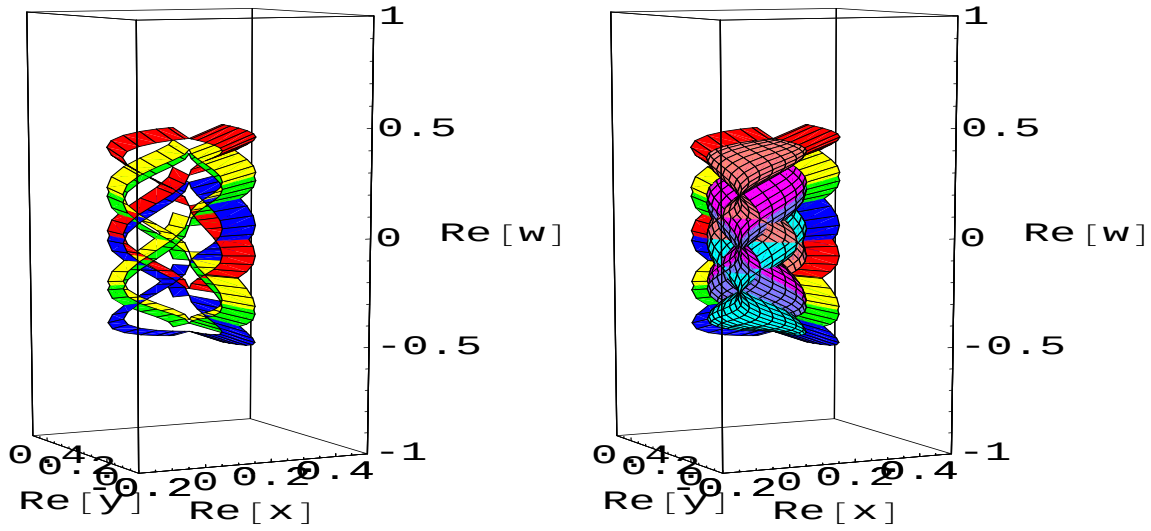

(a) (b)

Figure 27: (a) The block of four commutator strips surrounding one of the five corners of a single B_5 Pochhammer pentagon. (b) Filling in the remainder of the surface at one corner of the pentagon, giving four "handkerchief" surface areas filling the corresponding branched cover threading its way around the branch points in the Riemann surface.

N	$\frac{N(N-3)}{2} = \mathbb{R}\mathbf{P}$ dim.	$\frac{(N-1)!}{2}$ = no. components
4	2	3
5	5	12
6	9	60
7	14	360
8	20	2520
9	27	20160
10	35	181440

Table 2: The first column is the value of N for a given function B_N. The second column gives the dimension of the projective space that implements the blow-up in cross-ratio coordinates; this is the same as the number of faces of the polytope defined by the natural $u_{ij} = 0$ boundaries of the integration region for one component using the cross-ratio coordinates; these are not necessarily regular polytopes. The third column is the total number of components, i.e., the number of polytopes that fit together to give the analogs of the 5-crosscap dodecahedron for B_5.

---

of the $(N-1)!/2$ components is an $N(N-3)/2$-*polytope* — its (i,j)-th face is on the projective *hyperplane* given by $u_{ij} = 0$; these are not in general regular polytopes, but reflect the existence of various poles that correspond to multiparticle combinations in elementary spinless string theory. Table 2 summarizes for low N the number of cross-ratio variables appearing in the standard constraints, which is also the number of faces of the polytope defining a single component, along with the total number of components. These polytopes have an exact and previously unsuspected correspondence with the Stasheff associahedra [15–17], in all dimensions. Each of the B_6 components, for example, is a nonahedron, as pictured in Figure 28; this structure is described in detail by Devadoss [3], who also gives, for example, a tessellation of the moduli space $\overline{\mathcal{M}}_0^6(\mathbb{R})$ tiled by 60 nonahedral associahedra. Our work seems to indicate that the moduli spaces $\overline{\mathcal{M}}_0^N(\mathbb{R})$ studied by Devadoss can also be viewed as the space of N-point cross-ratios with the tessellations we have described in this paper.

We conjecture that the real integral form of B_N can always be expressed alternatively by a Pochhammer-like contour integral in the corresponding smooth complex algebraic variety M^c of dimension $(N-3)$ in $\mathbb{C}\mathbf{P}^{N(N-3)/2}$. The contour is a real $(N-3)$-dimensional submanifold and is obtained by wrapping copies of the $N(N-3)/2$-polytope integral domain properly around the branch hyperplanes

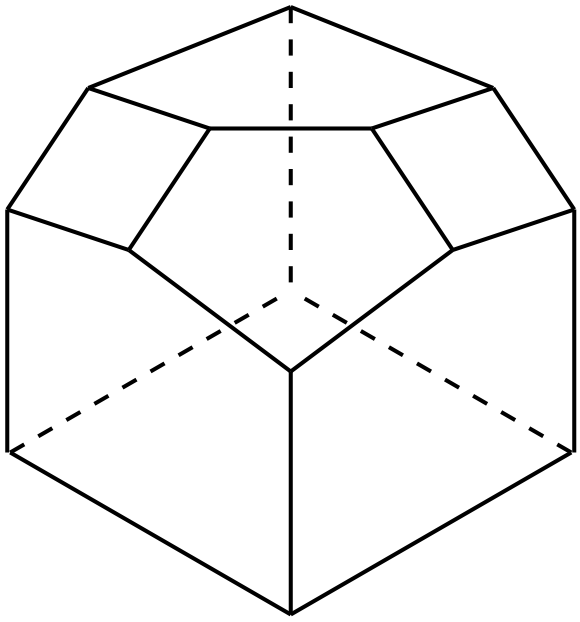

Figure 28: This nonahedron is the elementary connected component of the 6-point cross-ratios forming the basis for the analysis of B_6; just as 12 pentagons tessellate the 5-crosscap surface, 60 of these nonahedra tessellate the analogous 3-manifold.

where its faces are located. Notice that it is fairly easy to see, by the description above and (3), that the branch hyperplane at each face – say, face (i, j) – is of complex codimension 1 in M^c and, when folded around it, the *phase* of the integrand in the lift to the Riemann covering sheaf changes by $\pm\alpha_{ij}$. By this mechanism, (6) should generalize in an obvious way.

Acknowledgments

This research was supported in part by NSF grant numbers CCR-0204112 and IIS-0430730. AJH is grateful to Tullio Regge for his early encouragement and interest in this problem. Special thanks are due to Charles Livingston, Philip Chi-Wing Fu, and Sidharth Thakur for advice, insights, and assistance with graphics tools. We also thank James Stasheff for introducing us to the literature on associahedra.

References

[1] K. Bardakci and H. Ruegg. Reggeized resonance model for the production amplitude. *Phys. Letters*, 28B:342–347, 1968.

[2] H. R. Brahana and A. B. Coble. Maps of twelve countries with five sides with a group of order 120 containing an ikosahedral subgroup. *Amer. J. Math.*, 48(1):1–20, 1926.

[3] Satyan L. Devadoss. Tessellations of moduli spaces and the mosaic operad. In *Homotopy invariant algebraic structures. (Baltimore, MD, 1998)*, volume 239, pages 91–114, Providence, RI, 1999. Amer. Math. Soc.

[4] T. Goto. Relativistic quantum mechanics of one-dimensional mechanical continuum and subsidiary condition of dual resonance model. *Prog. Theor. Phys.*, 46:457, 1960.

[5] P. Griffiths and J. Harris. *Principles of Algebraic Geometry*. Wiley, New York, 1978. (See p. 184.).

[6] A. J. Hanson. Dual N-point functions in PGL(N-2,C)-invariant formalism. *Phys. Rev.*, D5:1948–1956, 1972.

[7] D. Hilbert and S. Cohn-Vossen. *Geometry and the Imagination*. Chelsea, New York, 1952.

[8] C. Jordan. *Cours d'analyse de l'Ecole Polytechnique*, volume 3. Gauthier-Villars, Paris, 1887.

[9] F. Klein. *Vorlesungen über das Ikosaeder und die Auflösung der Gleichungen vom fünften Grade*. Teubner, Leipzig, 1884. Reprinted Birkhäuser, Basel, 1993 (edited by P. Slodowy); translated as *Lectures on the icosahedron and the solution of equations of the fifth degree*, Kegan Paul, London, 1913 (2nd edition); reprinted by Dover, 1953.

[10] Z. Koba and H. B. Nielsen. Manifestly crossing-invariant parameterization of the n-meson amplitude. *Nucl. Phys.*, B12:517–536, 1969.

[11] Yoichiro Nambu. Duality and hydrodynamics, 1970. Lectures at the Copenhagen High Energy Symposium.

[12] L.A. Pochhammer. Zur theorie der Euler'schen integrale. *Math. Ann.*, 35:495–526, 1890.

[13] Joseph Polchinsky. *String Theory I.* Cambridge University Press, 1998.

[14] Joseph Polchinsky. *String Theory II*. Cambridge University Press, 1998.

[15] James Stasheff. Homotopy associativity of H-spaces. *Trans. Amer. Math. Soc.*, 108:275–292, 1963.

[16] James Stasheff. *H-spaces from a Homotopy Point of View*. Lecture Notes in Mathematics 161. Springer Verlag, New York, 1970.

[17] James Stasheff. What is . . . an operad? *Notices Amer. Math. Soc.*, 51(6):630–631, 2004.

[18] G. Veneziano. Dual resonance model. *Nuovo Cimento*, 57A:190, 1968.

[19] M. A. Virasoro. Generalization of Veneziano's formula for the five-point function. *Phys. Rev. Letters*, 22:37–39, 1969.

[20] M. Weber. Kepler's small stellated dodecahedron as a Riemann surface. *To appear in Pacific Journal of Mathematics*, 2005.

[21] E.T. Whittaker and G.N. Watson. *A Course of Modern Analysis*. Cambridge University Press, 1969. Republished from the original.